Innovation of Chemistry & Materials for Sustainability
Volume 2, Issue 2, July- Dec. **2025**
ISSN (Print): 3049 – 2548
ISSN (Online): 3049 – 0146
RESEARCH ARTICLE

Influence of Barium Titanate on Electrospun Piezoelectric and Non-Piezoelectric Polymer Nanofibers Toward Energy Harvesting Applications

Abhijit Pingal Sanga[a], Sajal Nandi[a], Sunanda Roy[b,c], and Barnali Dasgupta Ghosh[a]*

[a]Department of Chemistry, Birla Institute of Technology Mesra, Ranchi 835215, India.
[b]Mechanical Engineering, ACED, Alliance University, Bangalore, Karnataka 562106, India
[c]Mechanical Engineering, Inha University, 100 Inha-Ro, Incheon 22212, South Korea

*Correspondence: barnali.iitkgp@gmail.com; barnalidg@bitmesra.ac.in (B. Dasgupta Ghosh)

Abstract: The growing demand for self-powered and flexible electronics has drawn attention to piezoelectric materials, capable of converting mechanical energy into usable electricity. Piezoelectric polymeric materials have gained significant attention due to their unique ability to generate electrical signals in response to mechanical deformation, coupled with their lightweight, flexible, and biocompatible nature. These features make them promising candidates for next-generation energy harvesting systems, especially in wearable technology, biomedical implants, and self-powered sensing devices. In this work, we studied the effect of incorporation of barium titanate (BTO) nanoparticles on the electrospun Polyvinylidene Fluoride (PVDF) and Polyvinylpyrrolidone (PVP) for energy harvesting properties. For this, we prepare a piezoelectric polymer (PVDF/BTO) and a non-piezoelectric polymer (PVP/BTO) nanocomposite and compare their energy harvesting properties. BTO nanoparticles were synthesized using a sol-gel method and dispersed in polymer matrices via electrospinning. Detailed structural, thermal, and dielectric characterizations were performed alongside electromechanical testing. Among the systems, the PVDF/BTO nanocomposite demonstrated the highest energy harvesting performance, delivering an output voltage of 3.8 V, current of 2.1 µA, and power of 7.98 µW under cyclic mechanical stress. The PVP/BTO nanofibers, although a non-piezoelectric polymer, demonstrated a moderate output current (1.3 µA) and output voltage (2.4 V), revealing the influence of PVP's dipolar interactions, marking their promising auxiliary role in nanocomposite engineering. On comparison with a non-piezoelectric polymer matrix, there is an increase of 83% performance for PVDF/BTO nanocomposite. These results were attributed to enhanced β-phase formation and interfacial polarization of PVDF, facilitated by the BTO dispersion. This work illustrates the promise of interface-optimized hybrid nanofibers in enabling high-output, flexible nanogenerators for wearable and self-powered technologies.

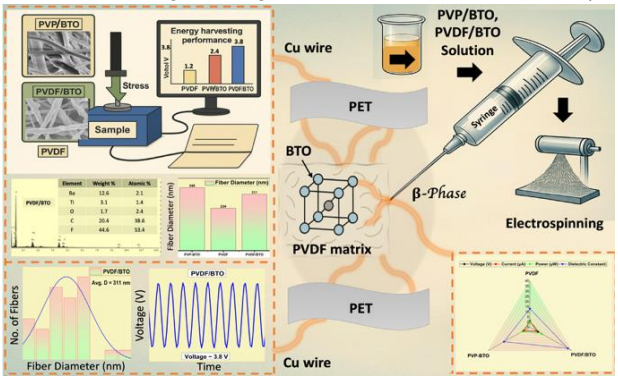

Keywords: *Electrospinning, barium titanate, polyvinylidene fluoride, polyvinylpyrrolidone, energy harvesting, piezoelectric nanogenerator*

1. Introduction

The continuous advancement of wearable electronics, wireless sensors, and implantable biomedical devices has heightened the need for flexible and efficient energy harvesting systems. As the era of smart and wearable electronics unfolds, the necessity for compact, sustainable energy sources has become increasingly prominent. Traditional batteries, though widely used, suffer from inherent limitations such as limited cycle life, rigidity and environmental concerns upon disposal. To overcome these challenges, researchers have turned towards energy harvesting technologies, particularly those that can harness ambient mechanical energy via the piezoelectric effect.[1] Hence, the piezoelectric energy harvesting has emerged as a promising approach due to its direct conversion of mechanical energy into electricity, even under low-frequency vibrations.

The growing need for compact, flexible, and self-sustaining electronic devices has garnered significant interest in developing piezoelectric nanogenerators (PENGs) using polymer nanofibers.[2] With advancements in electrospinning techniques, it is now possible to fabricate high-aspect-ratio fibers with precise control over crystal alignment, while incorporating functional fillers like BTO, ZnO, and graphene oxide to greatly enhance energy conversion efficiency.[3,4] Interestingly, recent research shows that even polymers without inherent piezoelectricity (non-piezoelectric polymer) can be engineered, either by introducing specially designed nanofillers or using advanced processing methods, to exhibit supplementary energy harvesting properties, which contribute to overall device performance.[5,6] Together, these innovations are driving polymer-based nanogenerators toward becoming promising solutions for applications such as wearable electronics, biomedical implants, and environmental energy harvesting.[7] Moreover, current reviews emphasize their scalability, multifunctional nature, and sustainability, making them strong contenders for next-generation energy devices.[8]

Barium titanate (BTO), a lead-free perovskite ceramic, exhibits a high dielectric constant and intrinsic piezoelectricity, making it an ideal additive to enhance the electromechanical response of PVDF. Hence, incorporating BTO nanoparticles into polymer matrices is an effective strategy for substantially enhancing the dielectric performance, boosting polarization and energy conversion efficiency.[9] Beyond dielectric improvement, BTO inclusion can also influence other critical material properties, including crystallinity, thermal conductivity, volume resistivity, rheological behaviour, curing characteristics, and mechanical strength.[10]

Among various piezoelectric materials, Polyvinylidene Fluoride (PVDF) has gained considerable attention as a promising polymer for energy storage and conversion systems due to its notable electroactive properties and excellent chemical stability.[11] In addition to its ferroelectric

https://doi.org/10.63654/icms.2025.02135 *Innov. Chem. Mater. Sustain.* **2025**, *2*(2), 135-150
Received: 15 July 2025; Revised: 21 August 2025; Accepted: 25 August 2025; Published (online): 05 September 2025

and piezoelectric behaviour, PVDF is also biocompatible, which has led to its successful application in biomedical devices such as pacemakers and wearable health monitoring systems.[12,13] Structurally, PVDF can crystallize into five distinct polymorphs-namely α, β, γ, δ, and ε- each exhibiting unique molecular conformations and physical properties. Among these, the β-phase is the most electroactive, characterized by an all-trans (TTTT) chain conformation that aligns the dipole moments in the same direction, thereby maximizing polarization. This makes β-phase PVDF particularly valuable for use in high-performance dielectric capacitors and piezoelectric devices.[14] Consequently, extensive research has been directed toward enhancing the β-phase content in PVDF. One of the most effective strategies to achieve this involves the incorporation of functional fillers, forming composite systems that facilitate phase transformation while also improving interfacial polarization. This approach is widely adopted due to its simplicity, scalability, and ability to fine-tune the electrical properties of PVDF-based materials. However, its performance is often hindered by the presence of non-polar α-phases and insufficient interfacial activity. To address these drawbacks, ceramic fillers such as barium titanate (BTO) have been introduced into PVDF matrices.

Again, Polyvinylpyrrolidone (PVP) has been utilized in this work, which serves a dual role as a non-piezoelectric polymer matrix and as a stabilizing agent to engineer BTO nanoparticles through an electrospinning route. Here, the electrospinning method has been utilized. This method not only eliminates the process of poling but also improves filler distribution and enhances dipole alignment, leading to improved electromechanical coupling.[15]

The electrospinning method aids in the alignment of BTO nanoparticles and promotes their interaction with PVDF chains, which in turn facilitates the formation of the electroactive β-phase. Formation of β-phase is crucial for enhancing piezoelectric performance and energy harvesting efficiency. Likewise, when BTO is combined with PVP during electrospinning, it helps to produce uniform nanofibers with a high aspect ratio, resulting in improved energy harvesting performance. To systematically explore the influence of piezoelectric BTO on the energy harvesting abilities, electrospun polymer nanofiber composites were prepared with PVDF and PVP.

In this work, we prepare a piezoelectric polymer (PVDF/BTO) and a non-piezoelectric polymer (PVP/BTO) nanocomposite and compare their energy harvesting properties. The BTO nanoparticles were synthesized using a sol-gel method and then uniformly dispersed in the polymer matrices through electrospinning. Structural, thermal, and dielectric characterizations were thoroughly carried out using techniques such as XRD, FTIR, and TGA/DSC. Electromechanical testing was also studied to assess their energy harvesting capabilities. A detailed analysis was conducted to examine the relationships among structure, interface, and output behaviour. This study offers valuable insights for designing next-generation, flexible, self-powered piezoelectric composites for efficient energy harvesting applications.

2. Experimental and preparation procedure

2.1 Materials

Polyvinylidene fluoride (PVDF), Thermo Fisher Scientific, India, Mw = 180,000 g/mol), polyvinylpyrrolidone (PVP) (CDH, Mw = 40,000 g/mol), Barium acetate (Fisher Scientific, India, 99%, Mw = 255.42 g/mol), titanium isopropoxide (Sigma Aldrich, India, 97%) were used as the raw materials for the synthesis of barium titanate (BTO) nanoparticles. HPLC grade

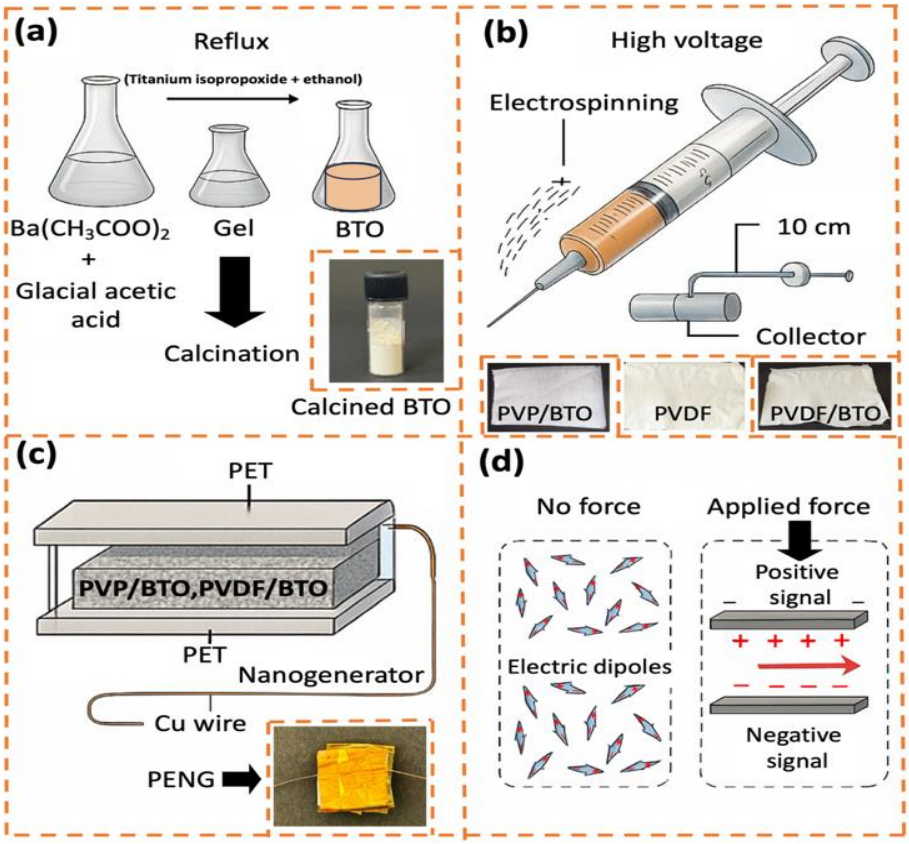

Figure 1. *Schematic representation of the (a) Synthesis of BTO nanoparticle (b) Fabrication of electrospun PVP, PVP/BTO, PVDF and PVDF/BTO nanofibers (c) Assembly of the flexible PENG and (d) Working principle of the nanogenerator under mechanical stress.*

dimethylformamide (DMF, Spectrochem, India, 99%, Mw = 73 g/mol) and acetone were procured from standard chemical suppliers (Sigma-Aldrich, India, 99%) and used without further purification. The DMF solvent was first purified by distillation, then treated using $CaCl_2$, and finally passed through 4Å molecular sieves. The raw components were dissolved using Glacial Acetic acid (Qualigens Fine Chemicals, 99.5%) and ethanol (Qualigens Fine Chemicals, 98%).

2.2 Synthesis of BTO Nanoparticles

BTO nanoparticles were synthesized via a sol-gel method using barium acetate and titanium isopropoxide as precursors. 0.1 moles of barium acetate ($Ba(CH_3COO)_2$), was dissolved in glacial acetic acid, while titanium isopropoxide was separately dissolved in ethanol under stirring, as illustrated in **Figure 1(a)**. The two precursor solutions were mixed dropwise and refluxed at 60 °C for 3 hours.[16] The resultant gel was dried at 100 °C and calcined at 900 °C for 3 hours, resulting in a white powder of highly crystalline BTO nanoparticles,[17] as shown in the inset image in **Figure 1(a)**. The BTO nanoparticles were thermally treated at 900 °C for 3 hours in a muffle furnace under ambient conditions. This step was crucial for eliminating any carbonaceous residues, such as acetate groups or solvent-derived residues, originating from the organic precursors (barium acetate, titanium isopropoxide, glacial acetic acid, and ethanol) in the sol-gel synthesis. The thermal treatment not only purifies the product but also helps to convert the initially amorphous material into a well-defined tetragonal perovskite structure, enhancing both the crystallinity and piezoelectric behaviour of the resulting BTO nanostructures.[18]

2.3 Preparation of Electrospun PVP Nanofibers

To fabricate neat PVP nanofiber via electrospinning, a 12 wt% solution of polyvinylpyrrolidone was prepared by dissolving the polymer in a 1:1 volume ratio of ethanol and N, N-dimethylformamide (DMF). This mixture was stirred magnetically for about 6 hours to achieve complete dissolution and homogeneity. The final electrospinning solution was loaded into a 10 mL syringe fitted with a 21-gauge metallic needle. Electrospinning was carried out at an applied voltage of 18 kV, with a flow rate of 1.5 mL/hour and a working distance of 10 cm between the needle tip and collector. The nanofibers were collected on aluminium foil and vacuum-dried at 60 °C for 12 hours to eliminate any residual solvents.

2.4 Preparation of Electrospun PVP/BTO Nanofibers

To prepare the electrospinning solution of PVP/BTO nanofiber, 0.0003 moles of PVP were first dissolved in a mixed solvent system comprising ethanol and DMF in a 4:1 volume ratio, followed by continuous magnetic stirring at room temperature for 3 hours until a homogeneous solution was obtained. Subsequently, 5 wt% of BTO nanoparticles were added into the PVP (12 wt%) solution and ultrasonicated for 30 minutes to ensure uniform dispersion before electrospinning.[19] The solution was then loaded into a syringe and electrospun under an applied voltage of 18 kV with a flow rate of 1.5 mL/hour and a tip-to-collector distance of 10 cm as depicted in **Figure 1(b)**. The resulting nanofibers were collected on aluminium foil, which was deposited as a nonwoven mat and vacuum-dried overnight.

2.5 Synthesis of PVDF Nanofiber

Neat PVDF nanofibers were prepared using the electrospinning technique. The PVDF polymer, with an average molecular weight of approximately 180,000, was used.[20] A uniform and viscous spinning solution was formulated using N, N-dimethylformamide and acetone, both of analytical grade. This solution was loaded into a 10 mL syringe and electrospun with a needle-to-collector distance of 10 cm. The process was carried out under an applied voltage of 18 kV, with a controlled flow rate of 1.5 mL/hour, with a rotating speed of 1100 rpm.

2.6 Preparation of electrospun PVDF/BTO composite films

For the composite variants, 5 wt% BTO nanoparticles were incorporated into the PVDF solution at concentrations of 12 wt% and uniformly dispersed using ultrasonication to prevent agglomeration.[21]

The prepared solutions were then subjected to electrospinning under optimized parameters. The electrospinning was performed by maintaining a 10 cm gap between the needle and collector, using an applied voltage of 18 kV. The solution was steadily delivered at a flow rate of 1.5 mL/h, while the collector rotated at a speed of 1100 rpm, the same as the process carried out for the synthesis of PVDF. The nanofibers were collected on a rotating drum to maintain uniformity in alignment and morphology. Finally, the electrospun films were thermally annealed at 80 °C for 2 hours to improve crystallinity and enhance phase formation in the PVDF matrix.

2.7 Fabrication of a sandwich-type flexible device

To fabricate the nanogenerator device, a 2 cm × 2 cm of electrospun nanofiber comprising either PVP/BTO or PVDF/BTO was sandwiched between conductive copper electrodes and encapsulated with PET films for mechanical robustness. Electrical connections were established by attaching copper wires to the electrodes using silver paste. To protect the device from environmental factors such as moisture and dust, the entire assembly was sealed with transparent Kapton tape, as shown in **Figure 1(c)**.

Figure 1(d) illustrates how the PENG operates. In its resting state-when no external pressure is applied, the dipoles within the piezoelectric layer are randomly arranged, and as a result, no electric potential is generated. Once a mechanical force is applied to the surface, these dipoles reorient in the direction of stress, causing a separation of charges and the development of an electric potential across the electrodes. To balance this potential, free charges from the external circuit flow toward the electrodes, creating a positive electrical output. When the pressure is removed, the dipoles gradually return to their initial, disordered orientation, causing the charge to flow in the opposite direction and produce a negative output signal.[22]

2.8 Characterizations

A series of advanced characterization techniques was employed to study the ceramic nanoparticles and polymer-based nanocomposite films. The Fourier Transform Infrared (FTIR) spectra were recorded using a Shimadzu IR-Prestige-21 instrument (Japan). The spectral range was 4000-400 cm^{-1} for the ceramics and 4000-600 cm^{-1} for the nanocomposite films in ATR mode. X-ray diffraction (XRD) patterns were collected using a Rigaku MiniFlex600 diffractometer utilizing Cu-Kα radiation (λ = 0.154 nm) to determine the crystalline structure and phase identification. The dielectric constant of the ceramic samples as a function of a frequency-dependent dielectric analysis ranging from 10 Hz to 10 MHz, was performed using a Novo-control ALPHA ATB impedance analyzer, which also provided information on capacitance across frequencies measured using a HIOKI 3532–50 LCR meter. For evaluating the surface topography and internal microstructure, a Sigma 300 field emission scanning electron microscope (FESEM) from Carl Zeiss, Germany, was used in conjunction with

energy-dispersive X-ray spectroscopy (EDS). A thin layer of platinum was sputter-coated onto the sample surfaces to enhance conductivity and imaging clarity. The thermal behaviour of the nanocomposites was studied using thermogravimetric analysis (TGA) and differential scanning calorimetry (DSC), conducted with TA Instruments Q10 (USA) and Shimadzu DTG-60 (Japan), respectively. The tensile behaviour of PVP, PVDF, PVP/BTO and PVDF/BTO composites was investigated using a universal testing machine (UTM, Tinius Olsen Bench-Mounted, Model 5ST) operated at a crosshead speed of 5 mm/min. The energy-harvesting performance of the composites was evaluated using a precision Source Meter Unit (SMU), Keysight B2900B/BL Series (USA).

3. Results and Discussion

3.1 Interface interaction of BTO within the polymer nanofibers

The schematic illustration shown in **Figure 2** represents the molecular-level interaction between BTO ceramic fillers and the β-phase PVDF polymer chains, which plays a crucial role in governing the piezoelectric response of the composite. PVDF is a polar polymer; its fluorinated backbone exhibits partial negative and positive charges. These charges are influenced by the electric field of the ferroelectric BTO particle. The electrostatic attraction between BTO's surface charges and PVDF's dipoles helps align the polymer chains into the energetically favourable β-phase during electrospinning.[9] Hydroxyl groups (-OH) commonly exist on the surface of BTO nanoparticles due to exposure to ambient conditions or synthesis in aqueous media.[23] These surface -OH groups can enhance interfacial interactions with polar polymer chains such as PVDF or PVP. Apart from electrostatics, dipole-dipole interactions arise between the permanent dipoles of PVDF and the polarized surface of BTO. This interaction promotes local ordering and facilitates conformational transition from α or γ phase to the electroactive β-phase. These interactions strengthen the local polarization field, leading to improved piezoelectric properties in the final nanocomposite. [24]

The surface of BTO features positively charged TiO_3 groups, which are naturally attracted to the negatively charged $-CH_2$ groups in PVDF. The filler acts as a nucleating center that influences the surrounding polymer chain arrangement.[25] This attraction encourages the PVDF chains to shift from their usual non-polar α-phase to the more desirable polar β-phase. The coloured atoms (fluorine in green, hydrogen in grey and carbon in black) represent the backbone of PVDF, emphasizing the dipolar character of each repeating unit ($-CH_2-CF_2-$).[26] The β-phase is important because it has a higher dipole moment, which greatly improves the material's piezoelectric and dielectric properties. However, to fully benefit from this effect, BTO nanoparticles must be evenly dispersed throughout the PVDF. As a result, the composite contains more β-phase PVDF, leading to a higher dielectric constant and a stronger piezoelectric response than pure PVDF alone.

3.2 X-ray Diffraction (XRD) Analysis

The crystalline structure and phase identification of the composite systems were examined using XRD. The sharp and distinct peaks observed at 2θ values of 31.5°, 38.9°, and 45.3° confirmed the presence of the tetragonal phase of BTO in all composite samples, indicating the successful retention of its perovskite structure during processing. In the case of neat PVDF and PVDF/BTO composites, a prominent diffraction peak around 20.6° was observed, which corresponds to the (110)/(200) planes of the electroactive β-phase. The inclusion of BTO nanoparticles clearly enhanced the β-phase content, as evidenced by the intensified peak at 20.6°. Meanwhile, PVP/BTO nanofibers exhibited relatively broadened peaks, a feature typically associated with nanoscale crystallinity and reduced grain size due to electrospinning-induced confinement effects.[27]

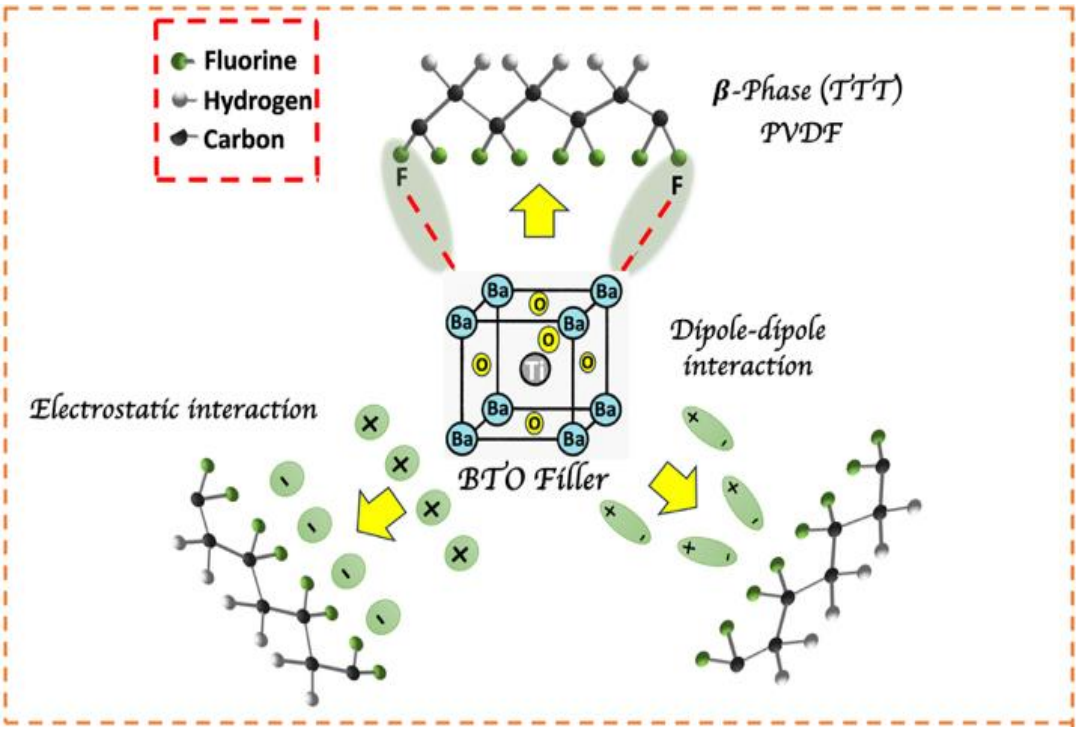

Figure 2. *A schematic illustration of the interfacial interaction mechanism between β-phase PVDF chains and BTO fillers.*

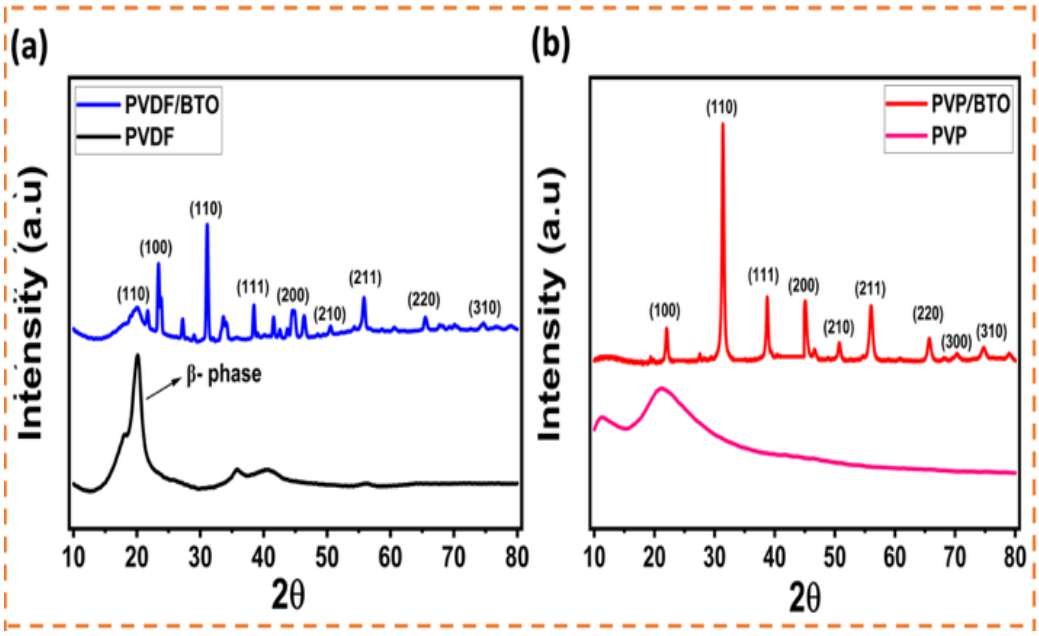

Figure 3. *(a) X-ray diffraction patterns of PVDF and PVDF/BTO nanocomposite fibres showing distinct peaks of BTO and the β-phase of PVDF, and (b) XRD pattern of PVP/BTO and PVP.*

Figure 3(a) shows the comparative X-ray diffraction (XRD) patterns of neat PVDF and PVDF/BTO nanocomposite fibers recorded in the 2θ range of 10° to 80°. The neat PVDF sample exhibits a broad diffraction peak around 2θ ≈ 20.6°, which is a characteristic fingerprint of the β-phase of PVDF. This polar phase is known for its piezoelectric and ferroelectric properties, crucial for energy harvesting applications. In contrast, the PVDF/BTO composite displays a set of sharp and well-defined peaks in addition to the β-phase peak of PVDF. These new peaks correspond to the perovskite structure of BTO with major reflections observed at 22.1° (100), 31.6° (110), 38.9° (111), 45.3° (200), and 51.1° (210) planes.[28] The incorporation of BTO not only introduces its intrinsic crystalline peaks but also slightly enhances the intensity and sharpness of the β-phase peak in PVDF, suggesting a synergistic effect that may help to stabilize the polar β-phase. The PVDF/BTO sample shows a relatively sharper and more intense β-phase peak compared to pure PVDF, which indicates improved phase crystallinity, likely induced by the nucleating effect of BTO nanoparticles. These ceramic fillers can act as nucleation center, facilitating the alignment of PVDF chains into the all-trans conformation required for β-phase formation.[29]

The neat PVP spectrum [**Figure 3(b)**] exhibits a broad and featureless halo centred around 20°, which is characteristic of its amorphous nature. This diffused pattern confirms the absence of any long-range order or crystalline domains in the pristine polymer matrix.

In contrast, the XRD pattern of the PVP/BTO composite [**Figure 3(b)**] displays a series of sharp and well-defined peaks, which can be unambiguously attributed to the crystalline phase of BTO. The most intense diffraction peak observed at 2θ ≈ 31.5°, along with additional reflections at 22.1°, 38.9°, 45.3°, 50.7°, and 56.2°, correspond well to the (100), (110), (111), (200), (210), and (211) planes, respectively, of the tetragonal perovskite BTO phase. The presence of these peaks confirms that the BTO nanoparticles retained their crystalline integrity even after incorporation into the PVP matrix via electrospinning.

Notably, the absence of any new peaks or significant shift in peak positions in the composite pattern indicates that no chemical interaction or phase transformation occurred during the fabrication process. Instead, the BTO crystallites appear to be physically embedded within the amorphous PVP network. The dominance of BTO peaks in the composite further suggests that the ceramic filler contributes prominently to the structural features of the hybrid nanofibers, while the PVP component serves primarily as a flexible polymeric support.

This result signifies successful fabrication of a hybrid nanocomposite where the functional inorganic BTO phase is well-dispersed within an amorphous polymer matrix, preserving its crystallinity and, by extension, its piezoelectric functionality.

The crystallite size of PVP/BTO and PVDF/BTO was calculated using the well-known Debye-Scherrer's equation (**Eq. 1**) and is shown in **Table 1**.

$$D = \frac{k\lambda}{\beta\cos\theta} \quad (1)$$

Where D is the average crystallite (nm), k is Scherrer's constant, typically taken as 0.9, λ is the wavelength of the X-ray source used (0.154 nm), β is the full width at half maximum (FWHM) of the diffraction peaks (radians), and θ is the Bragg angle corresponding to the peak position (radians). The average crystallite size for PVDF corresponds to 7.58 nm, for PVP/BTO is 27.4 nm and for PVDF/BTO is 32.5 nm, respectively.

Overall, the XRD results validate the successful incorporation of BTO within the PVDF matrix and its role in promoting the desirable β-phase for piezoelectric performance.

3.3 Fourier Transform Infrared Spectroscopy (FTIR) Analysis

Table 1. *Crystallite size of all three samples (PVP/BTO, PVDF/BTO and PVDF) calculated using Scherrer's equation.*

PVP/BTO				PVDF/BTO				PVDF		
2θ	(hkl)	FWHM (Radian)	Crystallite size (nm)	2θ	(hkl)	FWHM (Radian)	Crystallite size (nm)	2θ	FWHM (Radian)	Crystallite size (nm)
22.1	(100)	0.27	29.3	23.0	(100)	0.17	47.1	8.60	4.60	1.73
31.5	(110)	0.23	35.8	31.0	(110)	0.25	32.0	20.12	1.95	4.12
38.8	(111)	0.18	45.0	38.4	(111)	0.19	42.7	35.37	1.10	7.58
45.3	(200)	0.45	18.7	44.8	(200)	0.35	24.5	35.81	0.60	13.9
50.9	(210)	0.41	21.2	50.5	(210)	0.38	22.9	40.26	0.57	14.8
56.2	(211)	0.33	26.9	56.7	(211)	0.26	34.7	56.17	2.74	3.29
65.8	(220)	0.38	24.7	65.4	(220)	0.43	21.5			
70.3	(300)	0.36	27.0	70.5	(300)	0.27	36.0			
75.0	(310)	0.34	29.4	75.7	(310)	0.21	47.9			
79.4	(311)	0.63	16.23	78.9	(311)	0.66	15.5			

FTIR spectroscopy was employed to quantify and compare the β-phase content in the polymeric and composite nanofibers. The characteristic β-phase absorption bands near 840 cm^{-1} were distinctly visible in all samples. The fractional β content (*F(β)*) was acquired from FTIR using **Eq. 2**. In neat PVDF, the β-phase content was estimated to be approximately 60%, reflecting the baseline polarization of the polymer.[30] Upon embedding 5 wt% BTO nanoparticles, the β-phase fraction increased significantly to around 85%, suggesting that the ceramic fillers enhanced dipole orientation and induced a more ordered ferroelectric domain alignment, as it was summarized in **Table 2**.

$$F(\beta) = \frac{A_\beta}{1.3A_\alpha + A_\beta} \times 100 \qquad (2)$$

Where *F(β)* represents the fraction of the β-phase present in the sample, A_β which corresponds to the infrared absorption intensity at 841 cm^{-1} (associated with the β-phase), and A_α refers to the absorption at 769 cm^{-1}, which is characteristic of α-phase.

The FTIR spectra presented in **Figure 4(a)** confirm the successful incorporation of BTO nanoparticles into the PVDF matrix. In the case of PVDF and PVDF/BTO, characteristic absorption bands associated with the β-phase of PVDF were clearly observed at 1404 cm^{-1}, 1072 cm^{-1}, and 841 cm^{-1}. These bands, corresponding to CH_2 bending and CF_2 stretching vibrations, became more prominent upon the incorporation of BTO, indicating an enhancement in β-phase content. Such enhancement is typically attributed to the nucleating effect of the ceramic filler, which promotes the all-trans conformation of PVDF chains. Additionally, a reduction in the O-H stretching intensity around 3400 cm^{-1} in the composite suggests potential hydrogen bonding or interaction between residual -OH groups in PVDF and surface oxygen atoms of BTO. Neat PVDF displays characteristic absorption bands at 840 cm^{-1} and 1275 cm^{-1}, which correspond to the β-phase (all-trans conformation), crucial for piezoelectric

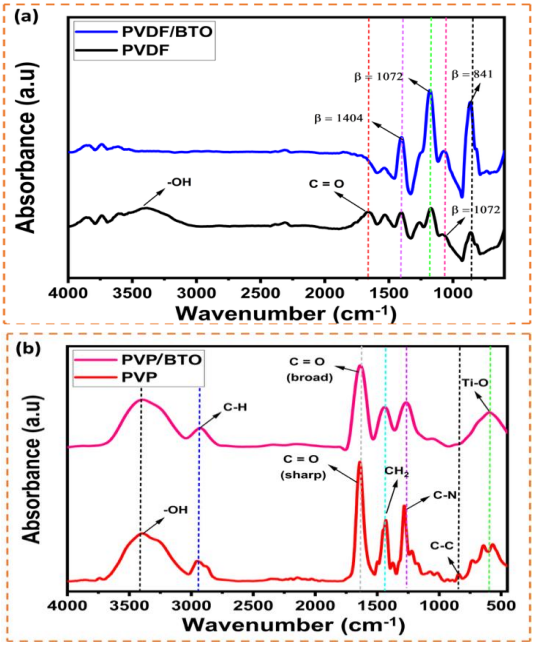

Figure 4. *FTIR spectra of (a) neat PVDF and PVDF/BTO nanocomposite showing prominent β-phase peaks and (b) PVP and PVP/BTO.*

behaviour.[31] A prominent peak at 1404 cm^{-1} further supports the β-phase dominance. In the composite (PVDF/BTO), these peaks become more defined and intense, indicating enhanced β-phase content due to the nucleating effect of BTO. Similarly, the FTIR spectrum of pure PVP-displayed distinct absorption peaks at 3435 cm^{-1} (O-H stretching), 2950 cm^{-1} (C–H stretching), and a sharp band at 1660 cm^{-1} corresponding to the carbonyl stretching (C=O) of the pyrrolidone ring [**Figure 4(b)**]. Upon introduction of BTO nanoparticles, the carbonyl peak broadened and exhibited a slight red shift, suggesting strong intermolecular interactions-likely coordination between the carbonyl group and Ba^{2+}/Ti^{4+} ions. Furthermore, a new broad band appeared in the 500-600 cm^{-1} range, which can be ascribed to Ti-O stretching

Table 2. *Summary of phase composition based on FTIR and XRD analysis for PVDF and PVDF/BTO.*

Sample	FTIR Peaks (cm^{-1})	Phase Identified (FTIR)	XRD Peak (2θ°)	Phase Identified (XRD)	β-Phase Content (%)
PVDF	840, 1275, 1404	β-phase dominant	20.6	β-phase	60
PVDF/BTO	840, 1275, 1404 (enhanced)	Strong β-phase	22.1, 31.6, 45.3	BTO + enhanced β-PVDF	>85

vibrations from the perovskite lattice of BTO. These spectral changes confirm successful incorporation of the ceramic phase and support the existence of robust interfacial interactions between PVP chains and BTO particles, which could contribute to the improved dielectric and electromechanical behaviour observed in the composite system.[32] This further confirms the composite formation and polymer-ceramic interactions.

3.4 Morphological Analysis

To investigate the surface morphology and fiber structure of the electrospun nanocomposites, FESEM analysis was employed. This high-resolution imaging technique provides detailed insights into the fiber diameter, uniformity, and nanoparticle dispersion within the polymer matrix. It is particularly valuable for evaluating the influence of ceramic fillers, such as BTO, on the electrospinning behaviour and nanostructure formation. The obtained micrographs help assess the effectiveness of nanoparticle integration and its correlation with the composite's functional performance. PVP/BTO fibers depicted homogeneous BTO distribution, while PVDF/BTO composites exhibited rougher textures due to embedded ceramic particles.[33] **Figure 5 (a-c)** displays the FESEM micrographs and corresponding fibre diameter distribution histograms. All samples were electrospun under optimized conditions to ensure uniform fiber formation. **Figure 5(a)** shows that the BTO nanoparticles were evenly distributed throughout the fibers, indicating a uniform and well-blended composite structure.[34] The average fiber diameter for PVP/BTO was approximately 348 nm, exhibiting a relatively broad distribution, which could be attributed to the incorporation of ceramic nanoparticles within the polymer matrix. This homogeneous dispersion is important because it ensures consistent properties across the material. In contrast, neat

PVDF fibers [**Figure 5(b)**] showed the thinnest and most uniform distribution with an average diameter of 234 nm, indicating smooth jet formation during electrospinning. This smooth morphology is typical for pure polymer nanofibers and serves as a useful reference point for comparing the effects of adding ceramic particles to the composite. **Figure 5(c)** illustrates the FESEM image of PVDF/BTO composite fibers, which revealed a noticeably rougher surface compared to the other samples. This increased roughness is directly linked to the presence of ceramic BTO particles, which are embedded within the polymer matrix. The mean diameter observed for the PVDF/BTO was 311 nm, slightly higher than neat PVDF. These particles disrupt the smooth surface of the PVDF fibers, resulting in a more textured appearance. Such surface roughness can influence the mechanical and functional properties of the fibers, potentially enhancing their performance in certain applications.

The EDS spectrum of the PVP/BTO nanofibers was depicted in **Figure 5(d)**. The corresponding elemental composition reveals dominant peaks for Ba (46.3 wt%), Ti (8.0 wt%), and O (21.7 wt%), confirming the presence of BTO in the composite. The presence of carbon (24.0 wt%) is due to the PVP polymer, and the high atomic percentage of carbon (51.8%) supports the organic-rich

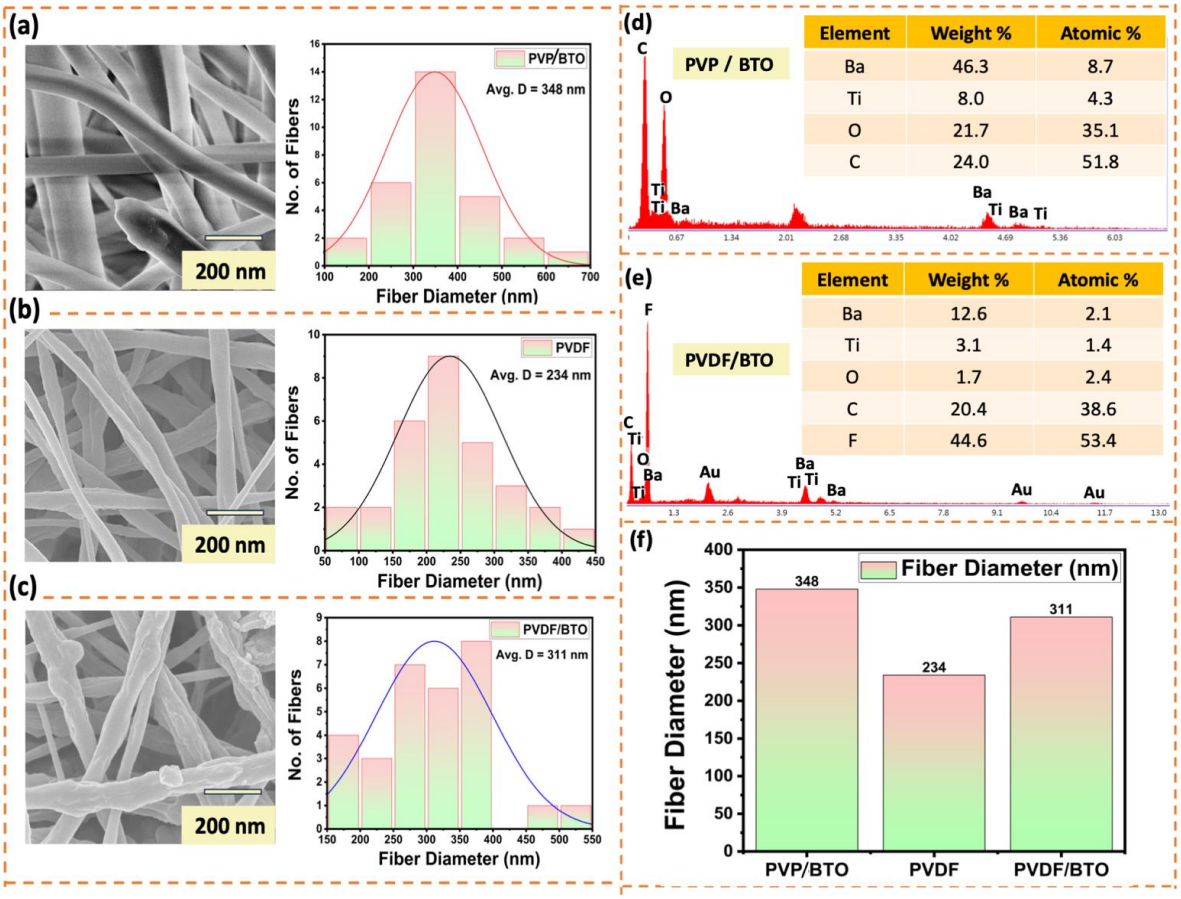

Figure 5. *FESEM images and corresponding fiber diameter distribution histograms of (a) PVP/BTO, (b) PVDF, and (c) PVDF/BTO nanofibers (d) EDS spectrum and elemental composition (weight % and atomic %) of PVP/BTO nanofibers confirming the presence of Ba, Ti, O, and C (e) EDS spectrum and elemental composition of PVDF/BTO nanofibers, highlighting the inclusion of BTO along with fluorinated PVDF matrix (f) Comparative bar graph of average fiber diameters for PVP/BTO, PVDF, and PVDF/BTO nanofibers.*

composition of the matrix. **Figure 5(e)** represents the EDS spectrum for PVDF/BTO nanofibers. The elemental composition confirms the successful inclusion of BTO, evident from Ba (12.6 wt%) and Ti (3.1 wt%), though at a significantly lower concentration compared to the PVP-based composite. The dominant presence of fluorine (44.6 wt%) corresponds to the PVDF matrix, which also contributes C (20.4 wt%) and O (1.7 wt%). The higher atomic percentage of F (53.4 wt%) reaffirms the fluoropolymer backbone of PVDF.

Figure 5(f) compares the average fiber diameters of the three nanofiber systems: PVP/BTO (348 nm), PVDF (234 nm), and PVDF/BTO (311 nm). The graphical representation underscores how the addition of BTO nanoparticles affects fiber morphology, with composites exhibiting higher average diameters compared to neat PVDF, consistent with increased solution viscosity and particle-polymer interactions during electrospinning.

Hence, the FESEM observations confirmed the successful fabrication of uniform, bead-free electrospun nanofibers across all sample systems. Neat PVDF exhibited the smallest and most consistent fiber diameter, while the inclusion of BTO nanoparticles in both PVP and PVDF matrices resulted in slightly thicker fibers due to increased viscosity and nanoparticle-polymer interactions. Among all, PVDF/BTO composites showed well-dispersed ceramic particles within the fibrous matrix, indicating strong filler-matrix compatibility and effective electrospinning. These morphological features are expected to enhance the composite's dielectric and piezoelectric performance.

3.5 Thermal Behaviour (TGA and DSC Analysis)

The thermal behaviour of the fabricated polymer-ceramic composites was thoroughly examined via DSC and TGA, which are essential tools for understanding polymer crystallization, degradation, and overall thermal stability. Additional relaxation peaks in the composite samples were indicative of enhanced crystallinity and improved phase distribution upon ceramic integration.

DSC thermograms shown in **Figure 6(a)** reveal key transitions associated with the melting and degradation processes of the individual and the thermal behaviour of PVP/BTO, PVDF, and PVDF/BTO composite systems, respectively. The PVP/BTO [**Figure 6(a)**] shows a broad endothermic peak between 400-800 °C, likely due to degradation of PVP and loss of absorbed water.[35,36] The PVP/BTO composite displayed a broader melting region at a slightly lower temperature range, characteristic of the semi-amorphous nature of PVP and its interaction with BTO. In neat PVDF**,** an endothermic peak appears around 170-180 °C, corresponding to its melting transition (T_m) related to the α-phase crystallinity. Incorporation of BTO nanoparticles within PVDF leads to a slight shift in T_m and a broader transition range, suggesting increased interaction at the filler-matrix.[37,38] The PVDF/BTO composite demonstrates enhanced thermal resistance and heat absorption, attributed to heterogeneous nucleation facilitated by ceramic particles, which is concordant with earlier findings,[39] it also shows a similar melting transition, but with slightly increased enthalpy and broader profile, suggesting an improved crystallization behaviour due to BTO acting as a heterogeneous nucleation site.

Thermogravimetric analysis revealed that all samples are thermally stable, affirming their suitability for practical applications involving elevated temperatures. TGA thermograms of the three samples are demonstrated in **Figure 6(b)**. Neat PVDF exhibits two-step degradation behaviour between 400-600 °C, typically attributed to chain scission and complete thermal decomposition.[9] The addition of BTO significantly altered the degradation profile.

The PVDF/BTO composite shows improved thermal stability compared to neat PVDF, likely due to the barrier effect of the dispersed ceramic particles, which retarded thermal degradation, also retaining more mass at higher temperatures, indicating the thermal shielding effect of BTO nanoparticles. The composite exhibits enhanced thermal stability (two-step thermal degradation), characterized by a delayed onset of degradation and a residue of nearly 60% at 600 °C. The residual weight indicates the presence of thermally stable BTO that enhances char formation and limits volatile evolution.[30,40] On the other hand, the PVP/BTO composite shows the earliest onset of weight loss due to the relatively lower thermal stability with decomposition of PVP and surface-absorbed moisture, with final residue consistent with ceramic content, yet retains more mass above 700 °C,

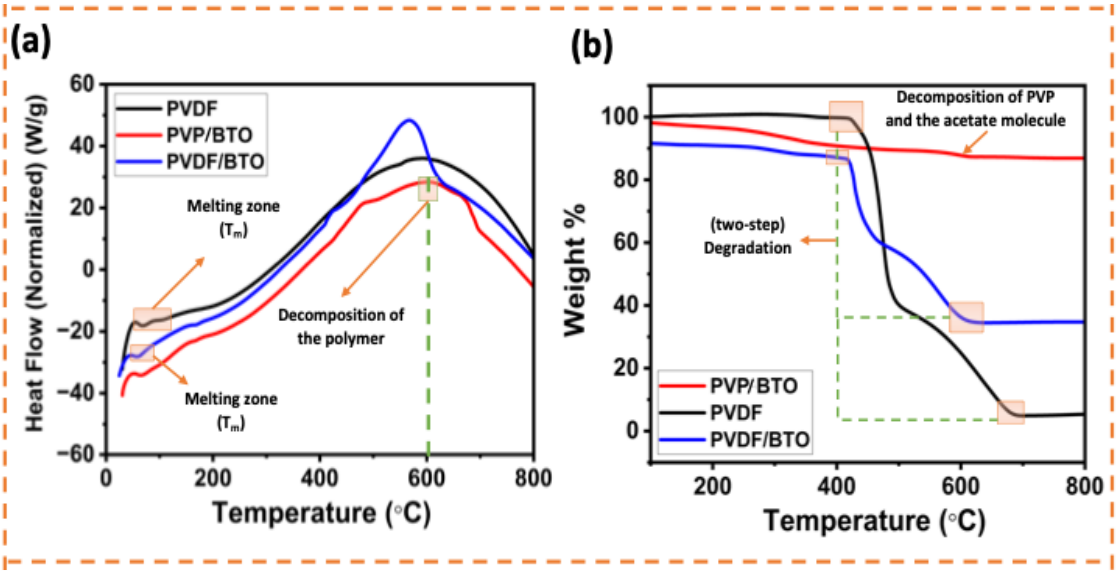

Figure 6. *DSC thermograms of (a) PVP/BTO, PVDF, PVDF/BTO, and TGA profiles of (b) PVP/BTO, PVDF and PVDF/BTO.*

which is likely due to the ceramic support structure and possible synergistic effects during combustion.[41,42]

These results confirm that BTO incorporation enhances both thermal and phase stability of the PVDF matrix, supporting its use in energy harvesting devices where heat resistance and structural integrity are crucial.

3.6. Mechanical Properties

Mechanical properties of the nanofibers were evaluated through tensile strength, elongation at break, and Young's modulus as illustrated in **Table 3**. Neat PVP displayed the lowest tensile strength (1.24 ± 0.39 MPa) and modulus (17.1 ± 5.19 MPa) with limited elongation (11.4 ± 0.72%), reflecting its flexibility but weak mechanical stability. In contrast, neat PVDF exhibited higher tensile strength (7.17 ± 1.11 MPa) and elongation (54.4 ± 23.8%) due to its semi-crystalline nature and stronger intermolecular interactions, resulting in greater stiffness (28.0 ± 2.18 MPa).

Adding BTO to PVP (PVP/BTO) moderately improved strength (2.79 ± 0.42 MPa) and stiffness (23.2 ± 9.93 MPa) but reduced elongation (5.90 ± 0.38%), as the rigid filler restricted chain mobility and increased brittleness. PVDF/BTO showed the most balanced performance, with tensile strength rising to 12.6 ± 2.60 MPa, modulus to 35.8 ± 8.26 MPa, and elongation improving to 60.6 ± 8.16%. These indicate uniform filler dispersion, strong interfacial adhesion, and effective stress transfer, while optimal filler loading and enhanced β-phase formation preserved chain flexibility and delayed crack propagation, yielding superior mechanical resilience.

The observed enhancement in elongation at break can be attributed to several synergistic effects. Firstly, well-dispersed BTO nanoparticles can act as stress transfer bridges, redistributing the applied mechanical load more uniformly throughout the PVDF matrix. This prevents premature crack initiation and propagation, allowing the polymer chains to undergo higher deformation before failure.[43] Secondly, BTO incorporation may induce β-phase formation in PVDF due to strong interfacial interactions between the ceramic surface and the polymer chains, leading to an increase in chain alignment and flexibility under tensile loading.[44] Moreover, at optimal filler content, BTO particles can restrict localized plastic deformation but still allow segmental chain mobility, creating a balance between stiffness and flexibility.

In **Figure 7(a)**, the stress–strain curve of PVDF/BTO shows a distinct balance of high tensile strength (12.6 MPa) and ductility (60.6% strain), indicating its ability to withstand large deformations before failure. The initial steep slope reflects elastic deformation, where stress is effectively transferred from PVDF chains to rigid BTO nanoparticles, enhancing stiffness. With increasing strain, the smooth, continuous rise without abrupt drops signifies stable plastic deformation and strong interfacial adhesion, which minimizes crack initiation and enables efficient energy dissipation.

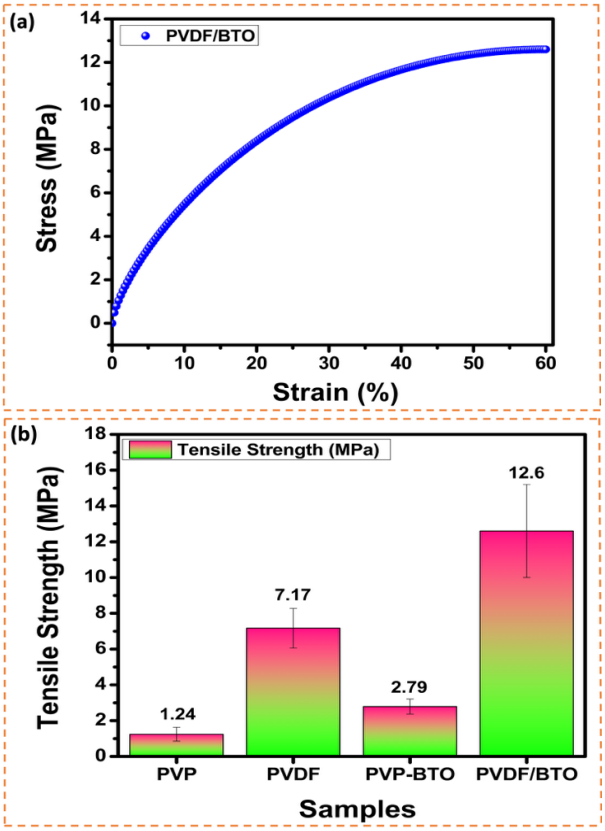

Figure 7. *(a) Stress–strain behaviour of the PVDF/BTO nanocomposite and (b) Tensile strength values of neat PVP, neat PVDF, PVP/BTO and PVDF/BTO nanocomposites.*

Figure 7(b) illustrates these trends, with tensile strength increasing from PVP to PVDF, and peaking in PVDF/BTO composites 75% higher than neat PVDF and over nine times higher than PVP, which is attributed to strong matrix–filler interactions enabling efficient stress transfer. Error bars represent standard deviations, confirming the reproducibility of results.

Such a mechanical profile, combining exceptional strength and stiffness with dimensional stability, makes these nanocomposites promising for high-performance applications, including flexible piezoelectric devices, structural reinforcements, and sensors where robust load-bearing capacity is essential.

3.7. Dielectric and Impedance Analysis

The dielectric response of the materials was examined over a wide frequency range, which is also a crucial tool for assessing the energy storage capabilities and polarization behaviour of polymer-based composites.

Table 3. *Summary of Tensile strength (MPa), Elongation at break (%) and Young's Modulus (MPa) for PVP, PVDF, PVP/BTO and PVDF/BTO nanofiber films.*

S.No.	Sample	Tensile strength (MPa)	Elongation at break (%)	Young's Modulus (MPa)
1.	PVP	1.24 ± 0.39	11.4 ± 0.72	17.1 ± 5.19
2.	PVDF	7.17 ± 1.11	54.4 ± 23.8	28.0 ± 2.18
3.	PVP/BTO	2.79 ± 0.42	5.90 ± 0.38	23.2 ± 9.93
4.	PVDF/BTO	12.6 ± 2.60	60.6 ± 8.16	35.8 ± 8.26

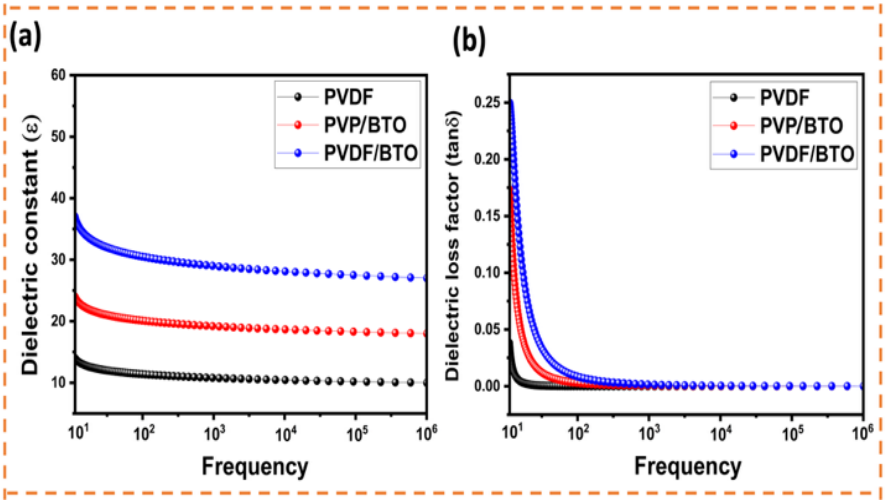

Figure 8. *(a) Frequency-dependent variation of dielectric constant (ε) for PVDF, PVP/BTO and PVDF/BTO composites (b) Frequency-dependent dielectric loss (tan δ) for the systems (PVDF, PVP/BTO and PVDF/BTO composites) measured at room temperature.*

Figure 8 illustrates the dielectric constant (ε) and dielectric loss (tan δ) as functions of frequency for PVDF, PVP/BTO and PVDF/BTO composites. As observed in **Figure 8(a)**, the dielectric constant for all samples decreases with increasing frequency, which is a typical dielectric dispersion phenomenon. At low frequencies (10^1-10^3 Hz), the polarization due to charge accumulation at interfaces (Maxwell-Wagner-Sillars effect) is more prominent, leading to higher dielectric constant values.[45,46] The PVDF/BTO exhibits the highest dielectric constant (36 at 10^1 Hz), significantly outperforming PVDF (ε = 13) and the PVP/BTO sample (ε = 23). Furthermore, electrospun PVP/BTO fibers also demonstrated a noticeable improvement in dielectric properties due to enhanced space charge polarization facilitated by the polymer matrix and the dispersed ceramic domains. In PVDF/BTO, this enhancement is attributed to the strong dipolar interactions between the polar PVDF chains and the high relative permittivity (k) of BTO nanoparticles, which facilitate better polarization.[47] Moreover, the incorporation of BTO improves the space charge polarization and interfacial interactions, resulting in superior dielectric permittivity. The synergistic interaction between polymer matrix and ceramic filler also restricts polymer chain mobility, promoting interfacial charge buildup.[48]

In **Figure. 8(b)**, the dielectric loss shows a steep decline with increasing frequency for all samples. The low-frequency region shows higher dielectric loss due to relaxation phenomena and conduction losses. Among the three, PVDF exhibits the lowest dielectric loss (0.036) throughout the frequency spectrum. While PVP/BTO and PVDF/BTO systems show slightly higher tan δ (0.169 and 0.25) at low frequencies, they stabilize to minimal values (0.01) at higher frequencies (>10^4 Hz), indicating the composite's suitability for energy storage or sensor applications where low loss at operational frequencies is critical.[49] The PVDF/BTO composite maintains a reasonable balance of high dielectric constant and low dielectric loss, making it a promising candidate for embedded capacitors and piezoelectric applications.[50]

3.8. Energy Harvesting Performance

The energy harvesting capability of the nanogenerators was investigated under low-frequency (2 Hz) cyclic compressive stress using the phenomenon of piezoelectricity. In general, piezoelectricity is the ability of certain materials to generate an electrical charge in response to applied mechanical stress.[51] This phenomenon is rooted in the non-centrosymmetric crystal structure of piezoelectric materials, where mechanical deformation leads to the displacement of charge centres within the material, inducing an electric polarization. The resulting piezoelectric effect can be exploited to convert ambient mechanical energy, such as vibrations, pressure, or motion, into usable electrical energy, making it ideal for self-powered sensors and energy-harvesting devices.[52]

In the context of our study, we employed the piezoelectric property to evaluate the dynamic electromechanical response of pure PVP, neat PVDF, PVP/BTO, and PVDF/BTO nanocomposite films. This was accomplished by applying cyclic mechanical compressive forces using a piezometer-based setup, which stimulated the materials and generated time-dependent voltage and current outputs. To evaluate the piezoelectric energy harvesting potential of the fabricated nanocomposites, we employed a piezometer-based dynamic mechanical testing system [**Figure 9(a)**]. Periodic compressive stress of 2 N pressure was applied to the composite films using the piezometer, which mimics mechanical stimuli like vibrations or footfall energy in practical scenarios. The resulting output current and voltage were recorded across all samples to assess their piezoelectric responsiveness.

The dynamic response of PVP, PVDF, PVP/BTO and PVDF/BTO films to cyclic loading was illustrated in **Figure 9(b-i)**. Although PVP is inherently non-piezoelectric, a weak alternating current (0.3 μA) and an output voltage of approximately 0.8 V were recorded [**Figure 9(b, c)**] when its nanofibers were subjected to mechanical deformation. This measurable output is likely attributed to the structural alignment of the fibers during electrospinning, which enhances dipolar orientation and enables modest charge separation under stress. PVDF exhibits a modest piezoelectric response, with a peak current of 0.5 μA and voltage of 1.2 V [**Figure 9(d, e)**]. This is consistent with the intrinsic piezoelectric nature of the β-phase PVDF polymer. [53,54] Incorporation of BTO nanoparticles into the PVP matrix significantly enhances the response, as seen in **Figure 9(f, g)**. The PVP/BTO nanofibers demonstrate a peak current of 1.3 μA and a voltage of 2.4 V. This enhancement can be attributed to the polarization of the ceramic fillers and the increased interfacial dipole

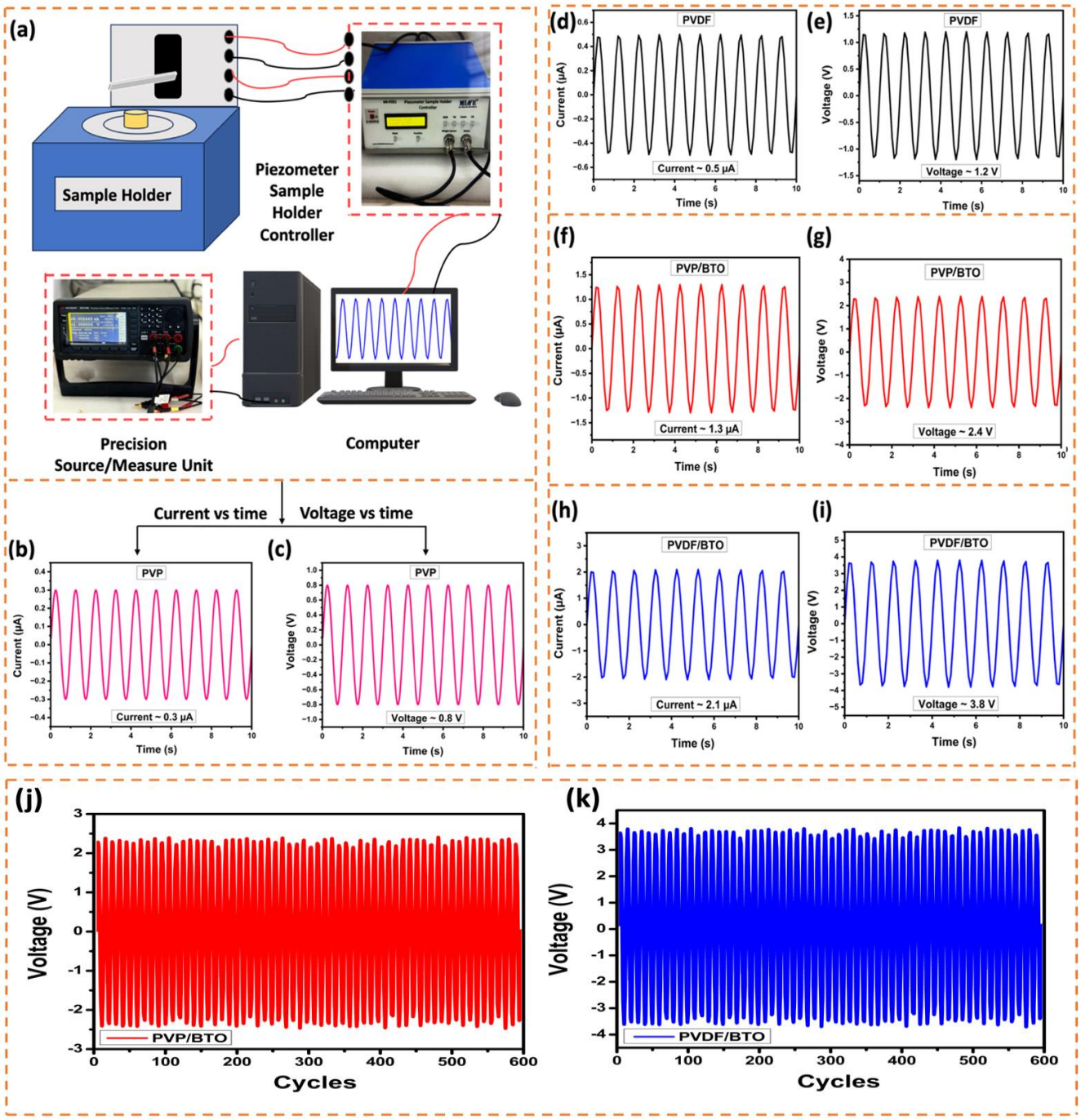

Figure 9. *(a) Schematic representation of the piezoelectric energy harvesting setup, (b-i) Output current and voltage profiles as a function of time for different samples under periodic mechanical stress at 2 Hz: (b) Current vs. time for PVP (c) Voltage vs. time for PVP (d) Current vs. time for PVDF, (e) Voltage vs. time for PVDF, (f) Current vs. time for PVP/BTO, (g) Voltage vs. time for PVP/BTO, (h) Current vs. time for PVDF/BTO, (i) Voltage vs. time for PVDF/BTO, and Durability test of : (j) PVP/BTO and (k) PVDF/BTO nanocomposite over 600 cycles through finger tapping.*

alignment, which collectively improve charge separation under mechanical excitation.[9] The most notable performance is observed when the 5 wt% of BTO nanoparticles were embedded in the PVDF matrix (PVDF/BTO composite), which achieves a maximum current output of 2.1 μA, and the output voltage surged to around 3.8 V [**Figure 9(h, i)**]. This significant improvement is attributed to the synergistic coupling of the polar β-phase PVDF matrix with highly dielectric BTO nanoparticles, which enhances dipole density and stress transfer at the interface.[55] We have also performed repeated finger-tapping tests, achieving over 600 cycles [**Figure 9(j, k)**] within a 10-minute span, which consistently demonstrated stable electrical output throughout the test period. These results suggest that our nanogenerator materials possess promising long-term operational stability. Due to limited access to advanced instrumentation, we were unable to conduct extended cyclic stability measurements beyond the presented data. Both composites demonstrated long-term stability and repeatability, but PVDF/BTO consistently produced higher voltages, underscoring its enhanced piezoelectric response.

Table 4. *General properties of electrospun PVP, PVP/BTO, PVDF, and PVDF/BTO composites for nanogenerator applications.*

Parameter	PVP	PVP/BTO	PVDF	PVDF/BTO Composite
Matrix	PVP	PVP	PVDF	PVDF
Filler	None	BTO (1-5 wt%)	None	BTO (1-5 wt%)
Synthesis Method	Electrospinning	Electrospinning	Electrospinning	Electrospinning
Interfacial Modifier	None	PVP	None	BTO nanoparticle
β-Phase Content	-	-	60%	>85%
Morphology	-	Uniform fibers with ceramic embedded	Smooth and thin nanofibers	Rougher fibers with well-dispersed ceramic
Thermal Stability	-	Moderate	High	Highest (T onset ↑ 20 °C)
Dielectric Constant (1 kHz)	-	23	13	36
Output Voltage (V)	0.8	2.4	1.2	3.8
Output Current (μA)	0.3	1.3	0.5	2.1
Output Power (μW)	0.24	3.12	0.6	7.98

A comparative study has been illustrated in **Table 4** to summarize the material's design, morphological characteristics, and output performance of these nanostructured systems: PVP, PVP/BTO, PVDF and PVDF/BTO composite nanofibers. The PVP/BTO system employed PVP both as the host matrix and as a surface-functionalizing agent for BTO nanoparticles, leading to uniform nanoparticle encapsulation. PVDF nanofibers served as the baseline with relatively high β-phase (60%) but limited output due to a lack of ceramic reinforcement.

In contrast, the PVDF/BTO composite nanofibers**,** fabricated by integrating BTO nanoparticles into a PVDF matrix, demonstrated the most favourable profile: a high β-phase content (>85%), dielectric performance (36 at 1 kHz), and energy harvesting output (3.8 V, 2.1 μA, 7.98 μW). This was made possible by improved ceramic dispersion, enhanced interfacial polarization, and effective dipole alignment under mechanical excitation.

The bar graph [**Figure 10(a)**] illustrates the maximum voltage output (V) generated by the PVP, PVDF, PVDF/BTO and PVP/BTO composite samples under periodic mechanical stress. Among them, PVDF/BTO exhibits the highest voltage output of 3.8 V, followed by PVP/BTO with 2.4 V, neat PVDF with 1.2 V and PVP nanofibers with only 0.8 V. This enhanced performance in PVDF/BTO can be attributed to the synergistic interaction between the ferroelectric BTO nanoparticles and the piezoelectric β-phase of PVDF, which collectively facilitate superior charge displacement and accumulation. The presence of BTO increases dipolar alignment, boosting the polarization field under dynamic compression.[56]

Figure 10(b) represents the output current (μA) generated under the same operating conditions. The PVDF/BTO composite again outperforms the others, reaching 2.1 μA, while PVP/BTO yields 1.3 μA, neat PVDF produces a current of 0.5 μA, and PVP nanofibers produce a significantly lower current of 0.3 μA. The improved charge mobility and dielectric interface between PVDF and BTO nanoparticles in the composite contribute to effective charge transfer during mechanical deformation. In contrast, the lower output from neat PVDF indicates a limited number of aligned dipoles and a lower β-phase content, resulting in a weaker piezoelectric response.[57]

The generated power of different nanocomposites was illustrated in **Figure 10(c)**. The power output was calculated using the following **Eq. (3)**:

$$P = V \times I \qquad (3)$$

The PVDF/BTO nanocomposite delivers a peak power output when load resistance (R=20 MΩ) is applied, which is approximately 7.98 μW, which is more than twice the output generated by PVP/BTO (3.12 μW), and significantly higher than both neat PVDF (0.6 μW) and PVP (0.24 μW), demonstrating its superior energy harvesting capability. These results highlight the critical importance of engineered dispersion of BTO within a neutral polymer like PVP, which can still elicit considerable piezoelectric-like response, demonstrating the role of filler orientation and dipolar polarization even without an electroactive polymer backbone. The composite structure enables more efficient conversion of mechanical energy into electrical energy through enhanced dielectric coupling and polarization.[58,59]

The comparative radar chart for the nanocomposites was depicted in **Figure 10(d)**, where it offers a comparative visualization of key performance parameters-voltage, current, power and dielectric constant, for the three sample types. PVDF/BTO exhibits dominant characteristics in all categories, forming a broad envelope in the radar plot, whereas PVDF appears more centrally clustered, reflecting its modest performance. PVP/BTO shows intermediate behaviour, suggesting a promising role but not surpassing PVDF/BTO. The radar plot effectively highlights the overall performance of the PVDF/BTO composites, demonstrating their strong potential for use in advanced piezoelectric nanogenerators and self-powered electronic applications. To further characterize the device performance, voltage and power density were measured across a range of load resistances through **Eq. (4):**

$$P = V^2 / AR \qquad (4)$$

Table 5. *Comparison of the piezoelectric output of our PVDF/BTO composite with that of other reported PENG devices.*

Sample	Fabrication Method	Current	Voltage (v)	Power Density (μWcm^{-2})	Reference
PMMA-BTO/PVDF-TrFE	Sol-gel + electrospinning	1.3 μA	12.6	0.68	63
PVDF/BTO	Electrospinning	-	11	0.65	64
BTO/PVDF-TrFE	Electrospinning	1.5 μA	6	0.878	65
PVDF/BTO/n-type graphene (n-Gr)	Sol-gel	1500 nA	10	-	66
$B_4Ti_3O_{12}$ nanoparticles	Spin-coating	100 nA	12.5	-	67
Electrospun PVDF nonwoven fabric	Electrospinning	39 nA	0.076	577.6	68
PVDF/BaTi(1-x)Zr_xO_3 (BTZO) film	Molten salt method	1350 nA	11.9	0.14	69
BTO NP/P(VDF-TrFE)	Drop-casting	82 nA	1.83	-	70
BTO/PVDF	Electrospinning	4.658 μA	62	3.64	71
SWCNTs/PVDF-TrFE	Electrospinning	1.3 μA	26.8	1.85	72
PVDF/BTO	**Electrospinning**	**2.1 μA**	**3.8**	**2.25**	**Our work**

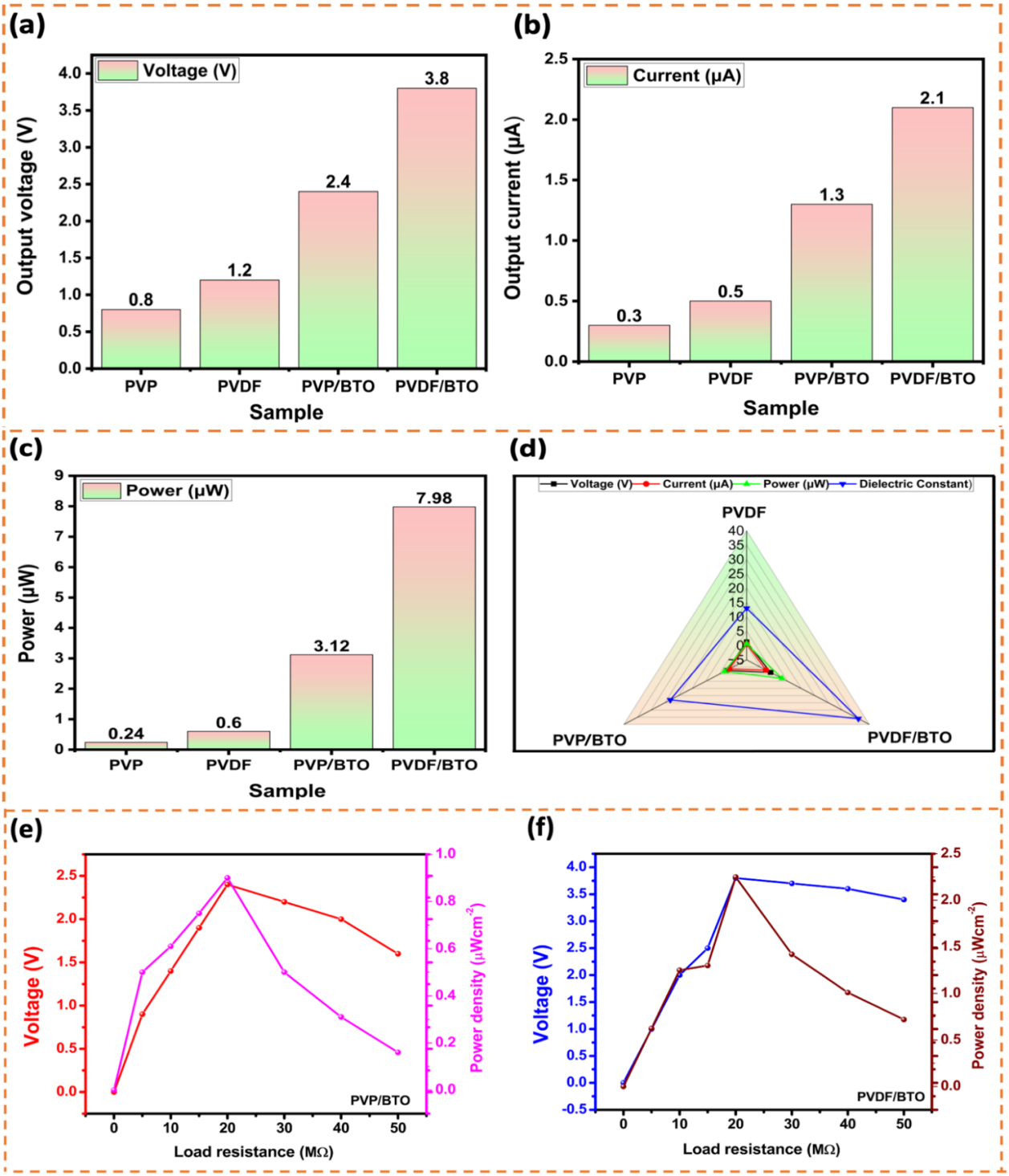

Figure 10. *(a) Comparative bar graph showing output voltage (V) of PVP, PVDF, PVP/BTO and PVDF/BTO nanocomposites under mechanical excitation using a piezometer setup, (b) Comparative bar graph showing output current (μA) from the four samples of (PVP, PVDF, PVDF/BTO, and PVP/BTO), (c) Power output (μW) derived from the voltage-current response, highlighting superior energy conversion efficiency in PVDF/BTO, (d) Radar chart representing multiple performance metrics-voltage, current, power, and dielectric constant-for PVDF, PVP/BTO, and PVDF/BTO composites and Voltage and power densities of (e) PVP/BTO and (f) PVDF/BTO nanocomposites with 0 to 50 MΩ load resistances.*

Both PVP/BTO and PVDF/BTO showed maximum output at intermediate resistances **Figure 10(e, f)**, but PVDF/BTO achieved significantly higher output voltage and power density of about 3.8 V and 2.25 μWcm^{-2} (area = 0.32 cm^2, R = 20 MΩ), confirming the beneficial effect of BTO integration in piezoelectric polymer. The observed improvements are a result of synergistic effects, including enhanced interfacial polarization, effective stress transfer, and improved filler dispersion in the polymer matrix.[60] These outcomes substantiate the potential of BTO-based composites for high-performance energy harvesting applications.[61,62]

As seen in **Table 5**, the PVDF/BTO composite achieves 3.8 V and 2.1 μA, outperforming several reported PENGs. This performance makes it a promising candidate for self-powered sensors, wearable electronics, and various miniaturized piezoelectric devices.

4. Conclusion

In this study, we investigated a comprehensive evaluation of electrospun nanocomposite fibers incorporating piezoelectric ceramic BTO into both PVDF and PVP polymer matrices, aiming to enhance energy harvesting performance. Accordingly, two types of nanocomposites were fabricated: piezoelectric PVDF/BTO and non-piezoelectric PVP/BTO, and their energy harvesting behaviours were systematically studied. A comprehensive comparison among PVP, PVDF, PVP/BTO and PVDF/BTO systems reveals that the PVDF/BTO composite achieves the highest performance in terms of dielectric constant (36 at 1 kHz), β-phase content (>85%), output power (7.98 μW) and power density (2.25 μWcm^{-2}), all under low-frequency mechanical excitation. This enhanced output is primarily due to the intrinsic piezoelectric properties of BTO, which acts as an active filler generating piezoelectric charges under stress, synergistically coupled with interfacial polarization effects between PVDF and BTO. The resulting strong dipole alignment not only stabilizes the β-phase of PVDF but also promotes uniform nanoparticle dispersion through electrospinning.

Thermal and morphological studies further support the structural integrity and reliability of these nanocomposites under stress. Although PVP (a non-piezoelectric polymer) lacks intrinsic piezoelectricity, its application as a host matrix in PVP/BTO nanofibers reveals valuable insights. It provides a benchmark to isolate filler contributions and supports controlled dispersion of BTO. The use of PVP not only stabilized BTO nanoparticles but also facilitated better values than the neat PVDF matrix.

These findings pave the way for the use of PVDF/BTO nanofiber composites as flexible and scalable materials for next-generation wearable piezoelectric nanogenerators. Their lightweight structure, mechanical robustness, and efficient energy conversion make them ideal candidates for integration into self-powered electronic systems, such as health-monitoring wearables, motion sensors, and ambient mechanical energy harvesters.

Supporting Information

The article contains all the information currently accessible.

Author Contribution Declaration

All the authors have made important contributions to the article.

Funding Sources

The Anusandhan National Research Foundation (ANRF), Government of India (Sanction order no. CRG/2022/001610) and NFST fellowship (Award No. 202223-NFST-JHA-02361).

Data Availability Declaration

The authors declare that the data supporting the findings are available within the article and properly cited.

Declaration of competing interest

The author declares that they have no known competing financial interests or personal relationships that could have appeared to influence the work reported in this paper.

Acknowledgement

B. Dasgupta Ghosh would like to acknowledge the funding received from the Anusandhan National Research Foundation (ANRF), Government of India, sanction order no. CRG/2022/001610 on “Electrospun PVDF based piezoelectric nanocomposite energy harvesters for self-powered smart wearable and implantable electronics.” A. Sanga acknowledges NFST for their fellowship (Award No. 202223-NFST-JHA-02361). The author would like to acknowledge Central Instrumentation Facility (CIF) at BIT Mesra, Ranchi, for analysis of the data.

References

1. C. Dagdeviren, Y. Su, P. Joe, R. Yona, Y. Liu, Y.S. Kim, Y. Huang, A. R. Damadoran, J. Xia, L.W. Martin, Y. Huang, J. A. Rogers. Conformable amplified lead zirconate titanate sensors with enhanced piezoelectric response for cutaneous pressure monitoring. *Nat. Commun*. **2014**, *5*, 4496. https://doi.org/10.1038/ncomms5496

2. Z. Wu, X. Ding, X. Chen, J. Chen, X. Chang, Z. Liu, L. Song, J. Huang, Y. Zhu. Recent progress of polymer-based piezoelectric nanogenerators. *Adv. Compos. Hybr. Mater*. **2025**, *8* 225. https://doi.org/10.1007/s42114-025-01225-0

3. M. Salama, A. Hamed, S. Noman, G. Magdy, N. Shehata, I. Kandas. Boosting piezoelectric properties of PVDF nanofibers via embedded graphene oxide nanosheets. *Sci. Rep.* **2024**, *14,* 16484. https://doi.org/10.1038/s41598-024-66258-9

4. K. Ren, Y. Shen, Z. L. Wang. Piezoelectric properties of electrospun polymer nanofibers and related energy harvesting applications. *Macromol. Mater. Eng.* **2024**, *309,* 2300307. https://doi.org/10.1002/mame.202300307

5. Y. Wang, L. Zhu, C. Du. Progress in piezoelectric nanogenerators based on PVDF composite films. *Micromachines* **2021**, *12,* 1278. https://doi.org/10.3390/mi12111278

6. J. Zidani, L. Tajounte, A. Benzaouak, N. Touach, A. Duong, M. Zannen, A. Lahmar. Advances in Lead-Free Flexible Piezoelectric Materials for Energy and Evolving Applications. *Adv. Ind. Eng. Polym. Res.* **2025**, *8*, 341. https://doi.org/10.1016/j.aiepr.2025.04.001

7. M. Kumar, S. Choudhary, S. K. Sharma, J. K. Randhawa. Piezoelectric nanogenerators with hybrid nanofibers: a dual approach for energy generation and wastewater treatment. *Environ. Sci.: Nano* **2025**,*12,* 1431. https://doi.org/10.1039/D4EN00568F

8. B. Mahanty, S. K. Ghosh, D. W. Lee. Advancements in polymer nanofiber-based piezoelectric nanogenerators: Revolutionizing self-powered wearable electronics and biomedical applications. *Chem. Eng. J.* **2024**, *495*, 153481. https://doi.org/10.1016/j.cej.2024.153481

9. B. J. Hansen, Y. Liu, R. Yang, Z. L. Wang. Hybrid nanogenerator for concurrently harvesting biomechanical and biochemical energy. *ACS Nano* **2010**, *4*, 3647. https://doi.org/10.1021/nn100845b

10. J. Su, J. Zhang, Recent development on modification of synthesized barium titanate ($BaTiO_3$) and polymer/$BaTiO_3$ dielectric composites. *J. Mater. Sci.: Mater. Electron* **2019**, *30*, 1957. https://doi.org/10.1007/s10854-018-0494-y

11. P. Martins, A. C. Lopes, S. Lanceros-Mendez, Electroactive phases of poly(vinylidene fluoride): Determination, processing and applications. *Prog. Polym. Sci*. **2014**, *39*, 683. https://doi.org/10.1016/j.progpolymsci.2013.07.006

12. C. M. Costa, V. F. Cardoso, P. Martins, D. M. Correia, R. Gonçalves, P. Costa, V. Correia, C. Ribeiro, M. M. Fernandes, P. M. Martins, S. Lanceros-Méndez. Smart and Multifunctional Materials Based on Electroactive Poly(vinylidene fluoride): Recent Advances and Opportunities in Sensors, Actuators, Energy, Environmental, and Biomedical Applications. *Chem. Rev.* **2023**, *123*, 11392. https://doi.org/10.1021/acs.chemrev.3c00196

13. S. Banerjee, Y. Patil, T. Ono, B. Ameduri. Synthesis of ω-Iodo and telechelic diiodo vinylidene fluoride-based (co)polymers by iodine transfer polymerization initiated by an innovative persistent

radical. *Macromolecules* **2017**, *50*, 203. https://doi.org/10.1021/acs.macromol.6b02308
14. A. Mukherjee, A. Ghosh, B. Dasgupta Ghosh. Fluoropolymer-Based Nanodielectrics for Energy Storage Application, Emerging Nanodielectric Materials for Energy Storage: From Bench to Field. Springer **2024**, 357–383. https://doi.org/10.1007/978-3-031-40938-7_13
15. K. Shi, B. Sun, X. Huang, P. Jiang. Synergistic effect of graphene nanosheet and $BaTiO_3$ nanoparticles on performance enhancement of electrospun PVDF nanofiber mat for flexible piezoelectric nanogenerators. *Nano Energy* **2018**, *52*, 153. https://doi.org/10.1016/j.nanoen.2018.07.053
16. A. Kumari, B. Dasgupta Ghosh. Effect of strontium doping on structural and dielectric behaviour of barium titanate nanoceramics. *Adv. Appl. Ceram.* **2018**, *117*, 427. https://doi.org/10.1080/17436753.2018.1491166
17. M. Maček Kržmanc, D. Klement, B. Jančar, D. Suvorov. Hydrothermal conditions for the formation of tetragonal BaTiO3 particles from potassium titanate and barium salt. *Ceram. Int.* **2015**, *41*, 15128. https://doi.org/10.1016/j.ceramint.2015.08.085
18. Y. Wei, Y. Song, X. Deng, B. Han, X. Zhang, Y. Shen, Y. Lin. Dielectric and ferroelectric properties of $BaTiO_3$ nanofibers prepared via electrospinning. *J. Mater. Sci. Technol.* **2014**, *30*, 743. https://doi.org/10.1016/j.jmst.2014.03.021
19. B. Sahoo, P. K. Panda. Preparation and characterization of barium titanate nanofibers by electrospinning. *Ceram. Int.* **2012**, *38*, 5189. https://doi.org/10.1016/j.ceramint.2012.03.025
20. Z. Li, J. Liao, Z. Xi, W. Zhu, Z. Zhang. Influence of Steric Hindrance on Ferro- and Piezoelectric Performance of Poly(vinylidene fluoride)-Based Ferroelectric Polymers. *Macromol. Chem. Phys.* **2019**, *220*, 1900273. https://doi.org/10.1002/macp.201900273
21. H. Güçlü, H. Kasım, M. Yazici. Investigation of the optimum vibration energy harvesting performance of electrospun PVDF/$BaTiO_3$ nanogenerator. *J. Compos. Mater.* **2023**, *57*, 409. https://doi.org/10.1177/00219983221144696
22. Q. Xu, J. Wen, Y. Qin. Development and outlook of high output piezoelectric nanogenerators. *Nano Energy* **2021**, *86*, 106080. https://doi.org/10.1016/j.nanoen.2021.106080
23. S. Wang, Z. Yu, L. Wang, Y. Wang, D. Yu, M. Wu. A core-shell structured barium titanate nanoparticles for the enhanced piezoelectric performance of wearable nanogenerator. *Appl. Energy* **2023**, *351*, 121835. https://doi.org/10.1016/j.apenergy.2023.121835
24. C. Lang, J. Fang, H. Shao, H. Wang, G. Yan, X. Ding, T. Lin. High-output acoustoelectric power generators from poly(vinylidenefluoride-co-trifluoroethylene) electrospun nano-nonwovens. *Nano Energy* **2017**, *35*, 146. https://doi.org/10.1016/j.nanoen.2017.03.038
25. A. J. Lovinger. POLY(VINYLIDENE FLUORIDE). *Jpn. J. Appl. Phys*., **1982**, *24*,18. https://doi.org/ 10.7567/JJAPS.24S2.18
26. A. K. Nandi, L. Mandelkern. The Influence of Chain Structure on the Equilibrium Melting Temperature of Poly (vinylidene fluoride). *J. Polym. Sci. Part B: Polym. Phys*. **1991**, *29*, 1287. https://doi.org/ 10.1002/polb.1991.090291012
27. D. Y. Lee, M. H. Lee, N. I. Cho, B. Y. Kim, Y. J. Oh. Effect of calcination temperature and atmosphere on crystal structure of $BaTiO_3$ nanofibers. *Met. Mater. Int.* **2010**, *16*, 453. https://doi.org/10.1007/s12540-010-0616-4
28. J. Yuh, L. Perez, W. M. Sigmund, J. C. Nino. Electrospinning of complex oxide nanofibers. *Phys. E. Low. Dimens. Syst. Nanostruct.* **2007**, *37*, 254. https://doi.org/10.1016/j.physe.2006.09.013
29. G. H. Kim, S. M. Hong, Y. Seo. Piezoelectric properties of poly(vinylidene fluoride) and carbon nanotube blends: β-phase development. *Phys. Chem. Chem. Phys.* **2009**, *11*, 10506. https://doi.org/10.1039/b912801h
30. S. Maensiri, W. Nuansing, J. Klinkaewnarong, P. Laokul, J. Khemprasit. Nanofibers of barium strontium titanate (BST) by sol-gel processing and electrospinning. *J. Colloid Interface Sci.* 2006, 297, 578. https://doi.org/10.1016/j.jcis.2005.11.005
31. R. Gregorio. Determination of the α, β, and γ crystalline phases of poly(vinylidene fluoride) films prepared at different conditions. *J. Appl. Polym. Sci.* **2006**, *100*, 3272. https://doi.org/10.1002/app.23137
32. B. Kim, Y. Jang, J. Kim, S. K. Kang, J. Song, D. W. Kim, S. Jang, I. Nam, P. S. Lee, S. H. Jeong. High-performance electrospun particulate matter (PM) filters embedded with self-polarizable tetragonal $BaTiO_3$ nanoparticles. *Chem. Eng. J.* **2022**, *450*, 138340. https://doi.org/10.1016/j.cej.2022.138340
33. M. Kubin, P. Makreski, M. Zanoni, L. Gasperini, G. Selleri, D. Fabiani, C. Gualandi, A. Bužarovska. Effects of nano-sized $BaTiO_3$ on microstructural, thermal, mechanical and piezoelectric behavior of electrospun PVDF/$BaTiO_3$ nanocomposite mats. *Polym. Test.* **2023**, *126*, 108158. https://doi.org/10.1016/j.polymertesting.2023.108158
34. X. Wang, X. Gao, M. Li, S. Chen, J. Sheng, J. Yu. Synthesis of flexible $BaTiO_3$ nanofibers for efficient vibration-driven piezocatalysis. *Ceram. Int.* **2021**, *47*, 25416. https://doi.org/10.1016/j.ceramint.2021.05.264
35. A. El Rahman, H. S. Metwally, N. Sabry, M. I. Mohammed. Gamma-ray shielding effectiveness, optical, mechanical, dielectric properties of nanofiller-reinforced PVA/PVP polymeric blend nanocomposites. *Sci. Rep.* **2024**, *14*, 27466. https://doi.org/10.1038/s41598-024-76397-8
36. K. Sreekanth, T. Siddaiah, N. O. Gopal, Y. Madhava Kumar, C. Ramu. Thermal, structural, optical and electrical conductivity studies of pure and Fe^{3+} ions doped PVP films for semoconducting polymer devices. *Mater. Res. Innov.* 2021, 25, 95. https://doi.org/10.1080/14328917.2020.1744346
37. R. Moriche, R. Donate, A. Otero, L. Santiago-Andrades, E. Monzón, M. J. Sayagués, M. Monzón, R. Paz. Processability and properties of cubic-$BaTiO_3$/poly(vinylidene fluoride) composites for additive manufacturing: From powder compounding to 3D-printed parts. *Polym. Compos*. **2024**, *46*, 7346. https://doi.org/10.1002/pc.29434
38. H. Ye, H. Chen, X. Zhang, Y. Chen, W. Shao, L. Xu. Electron structure in modified $BaTiO_3$/poly(vinylidenefluoride) nanocomposite with high dielectric property and energy density. *IET Nanodielectr.* **2019**, *2*, 70. https://doi.org/10.1049/iet-nde.2018.0029
39. M. Hirai, Y. Hagiwara, K. Takeuchi, R. Kimura, T. Onai, R. Kawai-Hirai, N. Tohta, M. Sugiyama. Thermal unfolding and refolding of protein under osmotic pressure clarified by wide-angle X-ray scattering. *Thermochim. Acta*. **2012**, *532*, 15. https://doi.org/10.1016/j.tca.2011.11.019
40. A. Bužarovska, M. Kubin, P. Makreski, M. Zanoni, L. Gasperini, G. Selleri, D. Fabiani, C. Gualandi. PVDF/$BaTiO_3$ composite foams with high content of β phase by thermally induced phase separation (TIPS). *J. Polym. Res.* **2022**, *29*, 272. https://doi.org/10.1007/s10965-022-03133-z
41. M. Elmowafy, K. Shalaby, M. H. Elkomy, O. A. Alsaidan, H. A. M. Gomaa, M. A. Abdelgawad, E. M. Mostafa. Polymeric Nanoparticles for Delivery of Natural Bioactive Agents: Recent Advances and Challenges. *Polym*. **2023**, *15*, 1123. https://doi.org/10.3390/polym15051123
42. R. Moriche, R. Donate, A. Otero, L. Santiago-Andrades, E. Monzón, M. J. Sayagués, M. Monzón, R. Paz. Processability and properties of cubic-$BaTiO_3$/poly(vinylidene fluoride) composites for additive manufacturing: From powder compounding to 3D-printed parts. *Polym. Compos*. **2024**, *46*, 7346. https://doi.org/10.1002/pc.29434
43. L. Yang, Q. Zhao, Y. Hou, R. Sun, M. Cheng, M. Shen, J. Qiu. High breakdown strength and outstanding piezoelectric performance in flexible PVDF based percolative nanocomposites through the synergistic effect of topological-structure and composition modulations. *Compos. -A: Appl. Sci. Manuf.* **2018**, *114*, 13. https://doi.org/10.1016/j.compositesa.2018.07.039
44. V. Fathollahzadeh, M. Khodaei, S. Emadi, K. Hajisharifi. Plasma-activated PVDF-$BaTiO_3$ composite nanofiber scaffolds loaded with vancomycin for enhancing biocompatibility and piezoelectric response. *Sci. Rep.* **2025**, *15*, 28515. https://doi.org/10.1038/s41598-025-14391-4
45. S. Shalu, P. Kar, J. Krupka, B. Dasgupta Ghosh. Synthesis, characterization, thermal, dynamic mechanical, and dielectric studies of $Ba_{0.7}Sr_{0.3}TiO_3$/polystyrene composites. *Polym. Compos*. **2018**, *39*, E1714. https://doi.org/10.1002/pc.24711
46. F. Deeba, K. Shrivastava, M. Bafna, A. Jain. Tuning of Dielectric Properties of Polymers by Composite Formation: The Effect of Inorganic Fillers Addition. *J. Compos. Sci.* **2022**, *6*, 355. https://doi.org/10.3390/jcs6120355

47. M. Serhan, M. Sprowls, D. Jackemeyer, M. Long, I. D. Perez, W. Maret, N. Tao, E. Forzani. Total iron measurement in human serum with a smartphone. In: 2019 AIChE Annual Meeting, Conference Proceedings. *Amer. Inst. Chem. Eng.* **2019**, *8*, 1-9. https://doi.org/10.1039/x0xx00000x
48. M. S. Zheng, C. Zhang, Y. Yang, Z. L. Xing, X. Chen, S. L. Zhong, Z. M. Dang. Improved dielectric properties of PVDF nanocomposites with core-shell structured $BaTiO_3$@polyurethane nanoparticles. *IET Nanodielectr*. **2020**, *3*, 94. https://doi.org/10.1049/IET-NDE.2020.0015
49. R. Bo, J. Liu, C. Wang, Y. Wang, P. He, Z. Han. Molecular Dynamics Simulation on Structure and Dielectric Permittivity of $BaTiO_3$/PVDF Composites. *Adv. Polym. Technol.* **2021**, *1*, 901. https://doi.org/10.1155/2021/9019580
50. Z. D. Liu, Y. Feng, W. L. Li. High Dielectric Constant and Low Loss of Polymeric Dielectric Composites Filled by Carbon Nanotubes Adhering $BaTiO_3$ Hybrid Particles. *RSC Advances* **2015**, *5*, 29017. https://doi.org/10.1039/C5RA00639B
51. O. Okhay, A. Tkach. Current Achievements in Flexible Piezoelectric Nanogenerators Based on Barium Titanate. *Nanomater*. **2023**, *13*, 988. https://doi.org/10.3390/nano13060988
52. A. Mukherjee, B. Dasgupta Ghosh, S. Roy, K. Lim Goh. Ultra strong flexible $Ba_{0.7}Sr_{0.3}Zr_{0.02}Ti_{0.98}O_3$/MWCNT/PVDF Nanocomposites: Pioneering material with remarkable energy storage for Self-Powered devices. *Chem. Eng. J.* **2024**, *488*, 151014. https://doi.org/10.1016/j.cej.2024.151014
53. A. Mukherjee, B. Dasgupta Ghosh. Synthesis of functionalized ZnO nanoflake loaded polyvinylidene fluoride composites with enhanced energy storage properties. *Polym. Compos*. **2023**, *44*, 2488. https://doi.org/10.1002/pc.27258
54. H. S. Mohanty, Ravikant, A. Kumar, P. K. Kulriya, R. Thomas, D. K. Pradhan. Dielectric/ferroelectric properties of ferroelectric ceramic dispersed poly(vinylidene fluoride) with enhanced β-phase formation. *Mater. Chem. Phys.* **2019**, *230*, 221. https://doi.org/10.1016/j.matchemphys.2019.03.055
55. J. Yan, Y. G. Jeong. High Performance Flexible Piezoelectric Nanogenerators based on $BaTiO_3$ Nanofibers in Different Alignment Modes. *ACS Appl. Mater. Interfaces* **2016**, *8*, 15700. https://doi.org/10.1021/acsami.6b02177
56. P. Thakur, A. Kool, N. A. Hoque, B. Bagchi, F. Khatun, P. Biswas, D. Brahma, S. Roy, S. Banerjee, S. Das. Superior performances of in situ synthesized ZnO/PVDF thin film based self-poled piezoelectric nanogenerator and self-charged photo-power bank with high durability. *Nano Energy* **2018**, *44*, 456. https://doi.org/10.1016/j.nanoen.2017.11.065
57. N. R. Alluri, B. Saravanakumar, S. J. Kim. Flexible, hybrid piezoelectric film ($BaTi_{(1-x)}Zr_xO_3$)/PVDF nanogenerator as a self-powered fluid velocity sensor. *ACS Appl. Mater. Interfaces* **2015**, *7*, 9831. https://doi.org/10.1021/acsami.5b01760
58. U. Yaqoob, A. S. M. I. Uddin, G. S. Chung. A novel tri-layer flexible piezoelectric nanogenerator based on surface- modified graphene and PVDF-$BaTiO_3$ nanocomposites. *Appl. Surf. Sci.* **2017**, *405*, 420. https://doi.org/10.1016/j.apsusc.2017.01.314
59. X. Li, Y. Wang, Y. Rao, X. Ma, Y. Yang, J. Zhang. Enhanced Energy Storage in PVDF-Based Nanocomposite Capacitors through (00l)-Oriented $BaTiO_3$ Single-Crystal Platelets. *ACS Appl. Mater. Interfaces* **2024**, *16*, 27785. https://doi.org/10.1021/acsami.4c04340
60. M. M. Alam, S. K. Ghosh, A. Sultana, D. Mandal. Lead-free $ZnSnO_3$/MWCNTs-based self-poled flexible hybrid nanogenerator for piezoelectric power generation. *Nanotechnol.* **2015**, *26*, 165403. https://doi.org/10.1088/0957-4484/26/16/165403
61. U. Yaqoob, G. S. Chung. Effect of surface treated MWCNTs and $BaTiO_3$ nanoparticles on the dielectric properties of a P(VDF-TrFE) matrix. *J. Alloys. Compd.* **2017**, *695*, 1231. https://doi.org/10.1016/j.jallcom.2016.10.250
62. A. Kumari, B. Dasgupta Ghosh. A study of dielectric behavior of manganese doped barium titanate–polyimide composites. *Adv. Polym. Tech.* **2018**, *37*, 2270. https://doi.org/10.1002/adv.21886
63. K. Shi, B. Chai, H. Zou, P. Shen, B. Sun, P. Jiang, Z. Shi, X. Huang. Interface induced performance enhancement in flexible $BaTiO_3$/PVDF-TrFE based piezoelectric nanogenerators. *Nano Energy* **2021**, *80*, 105515. https://doi.org/10.1016/j.nanoen.2020.105515
64. K. Shi, B. Sun, X. Huang, P. Jiang. Synergistic effect of graphene nanosheet and $BaTiO_3$ nanoparticles on performance enhancement of electrospun PVDF nanofiber mat for flexible piezoelectric nanogenerators. *Nano Energy* **2018**, *52*, 153. https://doi.org/10.1016/j.nanoen.2018.07.053
65. X. Guan, B. Xu, J. Gong. Hierarchically architected polydopamine modified $BaTiO_3$@P(VDF-TrFE) nanocomposite fiber mats for flexible piezoelectric nanogenerators and self-powered sensors. *Nano Energy* **2020**, *70*, 104516. https://doi.org/10.1016/j.nanoen.2020.104516
66. U. Yaqoob, A. I. Uddin, G. S. Chung. A Novel Tri-Layer Flexible Piezoelectric Nanogenerator Based on Surface- Modified Graphene and PVDF-$BaTiO_3$ Nanocomposites. *Appl.Surf. Sci.* **2017**, *405*, 420. https://doi.org/10.1016/j.apsusc.2017.01.314
67. N. P. M. J. Raj, N. R. Alluri, G. Khandelwal, S. J. Kim. Lead-Free Piezoelectric Nanogenerator Using Lightweight Composite Films for Harnessing Biomechanical Energy. *Compos. B Eng.* **2019**, *161*, 608. https://doi.org/10.1016/j.compositesb.2018.12.129
68. Z. H. Liu, C. T. Pan, L. W. Lin, J. C. Huang, Z. Y. Ou. Direct-Write PVDF Nonwoven Fiber Fabric Energy Harvesters via the Hollow Cylindrical near-Field Electrospinning Process. *Smart Mater. Struct*. **2014**, *23*, 025003. https://doi.org/10.1088/0964-1726/23/2/025003
69. N. R. Alluri, B. Saravanakumar, S. J. Kim. Flexible, Hybrid Piezoelectric Film ($BaTi_{(1-x)}Zr_xO_3$)/PVDF Nanogenerator as a Self-Powered Fluid Velocity Sensor. *ACS Appl. Mater. Interfaces* **2015**, *7*, 9831. https://doi.org/10.1021/acsami.5b01760
70. X. Zhou, K. Parida, J. Chen, J. Xiong, Z. Zhou, F. Jiang, P. S. Lee. 3D printed auxetic structure-assisted piezoelectric energy harvesting and sensing. *Adv. Energy Mater*. **2023**, *13*, 2301159. https://doi.org/10.1002/aenm.202301159
71. Y. K. Kim, S. H. Hwang, H. J. Seo, S. M. Jeong, S. K. Lim. Effects of biomimetic cross-sectional morphology on the piezoelectric properties of $BaTiO_3$ nanorods-contained PVDF fibers. *Nano Energy* **2022**, *97*, 107216. https://doi.org/10.1016/j.nanoen.2022.107216
72. K. Kim, S. Lee, J. S. Nam, M. Joo, B. Mikladal, Q. Zhang, E. I. Kauppinen, I. Jeon, S. An. Highly transparent and mechanically robust energy-harvestable piezocomposite with embedded 1D P(VDF-TrFE) nanofibers and single-walled carbon nanotubes. *Adv. Funct. Mater.* **2023**, *33*, 2213374. https://doi.org/10.1002/adfm.202213374